The momentum spectrum of mouns in large extensive air showers

A. B. Walton

THE MOMENTUM SPECTRUM OF MUONS IN LARGE EXTENSIVE AIR SHOWERS

by

A.B.WALTON, B.Sc.

A Thesis submitted to the University of Durham

In accordance with the Regulations for

the Degree of Master of Science

Department of Physics
University of Durham.

May, 1966.

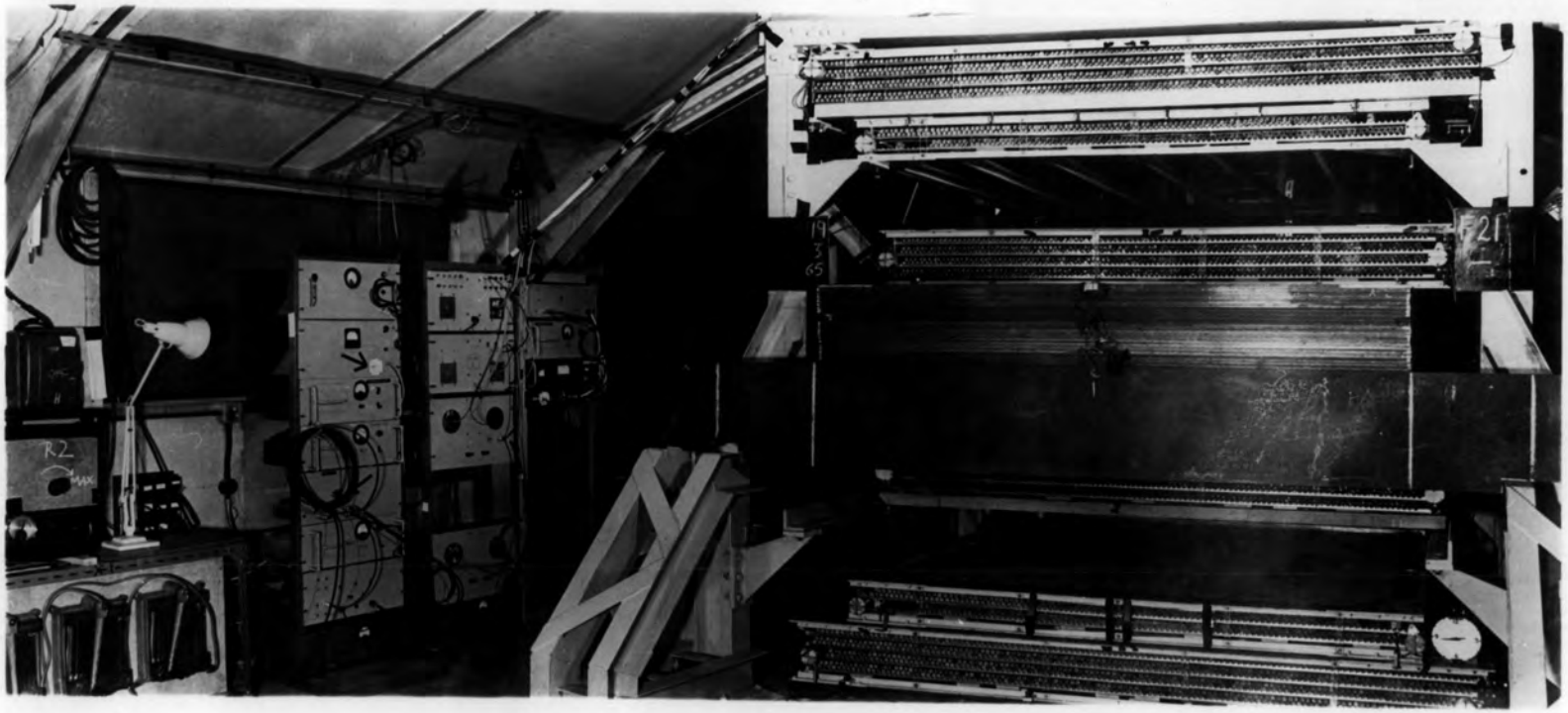
R2
19
3
65
F21

ABSTRACT

This thesis describes the construction and operation of a magnet spectrograph designed to measure the momentum spectrum of muons in Extensive Air Showers (EAS) detected by the three air shower arrays at Haverah Park near Harrogate.

The introduction contains a summary of the properties of air-showers and the various models of high energy interactions and cascade theories proposed to explain the observed phenomena. A survey of previous measurements on the momentum spectrum of muons in EAS is followed by an outline description of the present experiment and its aims.

The design and preliminary measurements carried out on the spectrograph are detailed in Chapter 2, together with the evaluation of the maximum detectable momentum, and the derivation of the acceptance function of the instrument.

The extensive air shower arrays, which detect showers with sizes from 10^5 to 10^8 particles, are described in Chapter 3, followed by a simplified form of air shower analysis, used for the smaller arrays.

Previous experiments using solid-iron magnets have relied on a relaxation method to derive the incident momentum spectrum, which is suitable only when a good approximation to the spectrum is known

beforehand. A second method of analysis is presented in Chapter 4, and the results are compared with the relaxation method. Good agreement is found.

Chapter 5 contains the preliminary results of the experiment, and a comparison with previous results and the predictions of theoretical models. Finally, an assessment is made of the future work judged to be most useful for comparison with the theoretical models.

PREFACE

This thesis describes the work done by the author, a research assistant in the Physics Department of the University of Durham, under the supervision of Professor G.D. Rochester F.R.S.

The magnet spectrograph was constructed by Professor G.D. Rochester, Dr. K.E. Turver and the technical staff of the Physics Department. The author took part in the loading of the neon flash tubes and the alignment and measurement of the flash tube trays. The preliminary zero-field run and the subsequent operation of the magnet were carried out by Dr. K.E. Turver and the author, who also assisted Professor A.J. Somogyi in the measurement of the magnetic field..

The small EAS arrays were designed by Dr. K.E. Turver. The author was largely responsible for their construction and calibration. The arrays were operated by Dr. K.E. Turver and the author and they were joined in September 1965 by Mr. J.C. Earnshaw and Mr. K.J. Orford.

Initial results were presented at the 9th International Conference on Cosmic Rays, London (September 1965), from the analysis by Professor A.J. Somogyi and Dr. K.E. Turver.

The author is entirely responsible for the second method of analysis of the data given in section 4-3. Mr. K.J. Orford provided

the computer programme for the test described in section 4-4, and Mr. J.C. Earnshaw carried out the calculations on the lateral distribution of muons in EAS, and the dependence of the muon densities on the shower size. The final calculations, described in Chapter five, were made by Dr. K.E. Turver and the author.

CONTENTS

CHAPTER 2 (contd.)

CHAPTER 5 (contd.)

CHAPTER 1

INTRODUCTION

1-1. The Extensive Air Shower

The extensive air shower is the result of a strong interaction between a high energy primary cosmic ray particle and an oxygen or nitrogen nucleus in the upper layers of the earth's atmosphere. The primary cosmic radiation falling upon the atmosphere consists of atomic nuclei of varying charge number, the most abundant being protons which are found with energies ranging from 10^8 to at least 10^{19} eV, those above 10^{13} eV being capable of initiating an EAS which is detectable at sea level. Heavy primary particles, with masses extending up to that of the iron nucleus, are thought to form only a small fraction of the primary flux up to 10^{13} eV (Waddington (1962)); this fraction is thought to increase at higher energies. (McCusker (1963)).

The number of mean interaction lengths for a nucleon in the atmosphere is 13, consequently the number of particles reaching sea-level without interacting is very small, and observations on the primaries must necessarily be made via their collision products. Apart from the number of primaries which interact before reaching sea-level, the rarity of such high energy particles compels an investigator to utilise the magnifying properties of the atmosphere to obtain a useful rate of detection with a comparatively small detector area.

1-1.1 General Characteristics of EAS

The particles in an extensive air shower are divided into three principal components: the nuclear-active component, the electromagnetic component and the muon component. The nuclear-active or N-component, comprising a strongly collimated beam of particles, the 'core' of the shower, is a direct result of the interaction, whilst the muon and electromagnetic components are the decay products of the nuclear-active particles. After the primary interaction, the N-component cascade is maintained by the interactions of the secondary nucleons, antinucleons, mesons and hyperons. The electromagnetic cascades are initiated by the decay of neutral pions into photons, whilst the muon component is formed by the decay of the charged pions and secondary kaons. The neutral pions, which give rise to the electromagnetic cascade, are produced in the primary interaction and to a lesser extent as the decay products of kaons and hyperons. A small contribution to the N-component is derived from high energy photons ($E_\gamma > 2$ GeV) which can generate pions through photonuclear interactions, which subsequently decay to muons. An opposing process, contributing to the electron-photon component, is the generation of electrons through the beta-decay and knock-on processes of muons. Both these cross-feeding processes may be ignored in a first approximation (Greisen (1960)).

1-1.2 The Electron-Photon Component

The electromagnetic component is the most abundant part of an EAS and it has been studied in great detail because of its importance

in the detection of air showers, although it does not have a close connection with the primary interaction. The processes involved in the formation of an electron-photon cascade are the energy loss of the electrons by bremsstrahlung and ionization, and the energy loss of the photons by pair production and the Compton effect. The bremsstrahlung radiation forms the main energy loss of the electrons above the critical energy E_c (84 MeV in air), since collision losses, including ionization of atoms and the production of δ-rays and knock-on electrons, are small and may be neglected. The most important energy loss for photons above the critical energy is pair production by the materialisation of δ-rays in the Coulomb field of a nucleus. The Compton effect is important only when considering energies below E_c, and plays no part in the formation of a shower.

Two approaches to the construction of a theoretical model for the longitudinal development of an electromagnetic cascade have been evolved. The method of successive collisions, due to Bhabha and Heitler (1937), is important for the early development of the shower, whilst the alternative approach, that of Carlson and Oppenheimer (1937), involving the solution of a set of diffusion equations, is more applicable to older showers. In the Carlson - Oppenheimer method, a set of differential equations is used to represent the change of the electron-photon energy spectrum with the thickness of absorber traversed and for a solution of the equations, certain simplifications must be made. Under Approximation A, in which the ionization loss of the electrons and the Compton effect of

the photons are neglected, a complete solution is possible (see eg. Janossy and Messel (1951)). Approximation B involves the addition of the ionization loss of the electrons, and a complete solution is not available (Snyder (1949)).

It is possible to ignore the effects of the lateral spread when considering the longitudinal development of an air shower, since the major cause of the lateral spread of the electron component is the multiple Coulomb scattering, which is large (0·2 radians for a 100 MeV electron in one radiation length) compared with the angular separation of a pair of electrons originating by pair production (0·005 radians for a pair of 100 MeV electrons). The complexity of any consideration of the scattering of the cascade particles is increased by the large range of electron and photon energies to be considered, and their dependence on the atmospheric depth.(see eg. Euler and Wergeland (1940), Molière (1946), Nishimura and Kamata (1950, 1951, 1952)). An empirical relation, representing the Nishimura and Kamata distribution for showers of age parameter s between 0·5 and 1·5 has been derived by Greisen (1960) and is

$$f\left(\frac{r}{r_1}\right) = \left(\frac{r}{r_1}\right)^{s-2} \left(1+\frac{r}{r_1}\right)^{s-4\cdot5} c(s)$$

where c(s) is tabulated by Greisen for values of s between 0·5 and 2·0. The age parameter s is zero at the start of the cascade, unity at the point of maximum development, and reaches a value of 2 when the cascade dies away to one particle. The density of particles at

distance r from the shower core is then given by

$$\triangle(r) = \frac{N}{r_1^2} \quad f\left(\frac{r}{r_1}\right)$$

where N is the total number of particles, and r_1 is the characteristic radius, or Molière scattering length, and is 79m in air at sea-level. This theoretical function with s = 1·25 and an additional term for the contribution from the mu-mesons and their secondary electrons has been found to be indistinguishable from the average experimental distributions for all charged particles, obtained by many workers, for shower sizes in the range 2×10^3 to 2×10^9 particles, atmospheric depths of 537gm cm^{-2} to 180gm cm^{-2}, and distances of a few metres to 1500 metres from the shower axis. The close agreement between all experiments and the theory with a constant age parameter can be explained by a continued infusion of energy into superimposed electromagnetic cascades due to the decay of the neutral pions produced by the interactions of the nuclear-active particles in the shower core. The thorough investigation of the longitudinal development of the electron-photon component has not been undertaken because of the difficulty of sampling an EAS at more than one level, though recently developed radio-Cerenkov techniques may now provide the experimental method.

1-1.3 The Nuclear-active Component

The nuclear interacting component of the EAS is more interesting because of its close relation with the primary collision, but is far more difficult to detect, due to its small abundance.

Very few measurements of this component have been made in large EAS, and consequently comparisons with theoretical predictions, based on models of meson cascade, are difficult.

The theories for meson production in high energy interactions may be divided into "one-centre" and "two-centre" models. In the one-centre model, treated by Fermi (1950), Landau (1953), and Heisenberg (1952), the nucleon - nucleon interaction is taken to be a single system until the meson emission has ended. Energy from the collision is considered to be statistically distributed throughout the new particles; in the Fermi and Landau treatments the original nucleons are included in the statistical distribution of energy, while in the Heisenberg theory the nucleons are allowed to escape before the equilibrium state is reached. Due to the inclusion of the original interacting nucleus in the partition of energy, the Fermi and Landau models predict an inelasticity close to unity. The treatments also regard a nucleon - nucleon collision as unique, yielding a fixed value for the multiplicity and angular anisotropy of the secondaries, which is incompatible with the wide variations found experimentally. From Heisenberg's treatment, the inelasticity is found to vary very strongly with the impact parameter of the collision, the Lorentz contraction of the meson clouds resulting in the localisation of the interaction energy in the volume of each field which actually overlaps. In this model, the proportion of the energy radiated as pions is given by the fraction of the interaction volume to the total volume of the two pion fields, hence the average value of the fractional energy

converted into pions falls with increase in the primary energy. The theory also predicts constant transverse momentum for the pions, and isotropy of the low energy particles in the CM system, both of which are observed experimentally. On the other hand, the treatment gives a dependence of the elasticity on the number of mesons created, which is not observed, and it fails to account for those events exhibiting a strong backward-forward peaking in the CM system.

The two-centre model of Kraushaar and Marks (1954) treats the collision as the separate excitation of each nucleon, which subsequently decay by evaporation of mesons, the number depending on the degree of excitation. This is in turn dependent on the relative momenta of recoil of the nucleons in the collision compared with their initial momenta, and consequently high excitation energies result from inelastic collisions. If few mesons are produced, the nucleons carry most of the energy, and a strong anisotropy of the secondaries should be observed. The experimentally observed degrees of anisotropy require the mass of the excited nucleus to be many times the nucleon rest mass and the inelasticity close to unity. If the meson cloud surrounding each nucleon is postulated to break away and trail behind with a lower velocity, as proposed by Cocconi (1958), and Ciok et al (1958), the difficulty may be overcome. The isotropic evaporation process for the meson fields proposed by Fermi is then able to account for the angular distributions in many of the jet events not represented in other models.

The Cocconi, Koester and Perkins (1961) model of nuclear interactions is based upon a set of empirical rules suggested by the available experimental data. The characteristics of the pion and proton fluxes from high energy interactions of protons with light nuclei were predicted using two separate approaches. The first method involves postulating a pion or proton energy spectrum in the laboratory system and combining this with the transverse momentum distribution to obtain an analytical expression for the pion flux. The second method results in an expression for the laboratory momentum spectrum from the combination of an assumed exponential longitudinal momentum distribution. Agreement between the two methods appears to be good, and also between the theory and experiment over the range of energies where comparison is possible.

Other approaches to the nucleon - nucleon collision have been concerned solely with the application of the theoretical predictions to EAS. Because of the complexity of the phenomena, great simplification is required, and only a qualitative comparison may be obtained between theory and observation. Messel (1954) extended the earlier work of Messel and Potts (1953), for cascades in a dense absorber, to penetrating showers in air, using a fixed primary energy. The theory ignores the possibility of further interactions of the charged pions during the subsequent cascade and consequently derives values for the muon to electron-photon component and muon to nuclear-active component ratios which are too large: Rozental (1952), again using a fixed primary energy, proposed a

model in which only the forward emitted particles in the CM system are considered. The number of particles produced is similar to the Fermi model. The relative number of particles as a function of atmospheric depth, and the lateral distribution function were also derived. Zatsepin (1956) compared the theory with experiment, but was unable to find satisfactory agreement. Zatsepin (1960) also proposed a model which assumed partial inelasticity and a resulting small change in the properties of EAS, due to the constant feeding of energy to the electromagnetic component. The calculations of Zatsepin predict that one particle carries off most of the interaction energy, and that, because of the low inelasticity, large fluctuations should occur in the shower development. The observed features of a shower detected are thus greatly dependent on the observation level, and the shower size is not uniquely related to the primary particle energy.

The Phenomenological Model of Ueda and McCusker (1962) is an attempt to explain the change in slope of the γ-ray spectrum at energies of 1,000 GeV, and the discontinuity in the slope of the EAS density spectrum. The model uses the cascade theory of Fukuda, Ogita and Ueda (1959), with several hypotheses on the pion energy distribution, assuming a primary energy spectrum composed entirely of protons. Good agreement with experiment has been obtained, and the model predicts many of the observed characteristics of EAS.

The calculations of Hillas (1966) are based on an assumed energy spectrum and angular distribution of secondaries from pion -

-nucleus collisions radiating the same pion energy as in the similar nucleon - nucleon collision. The meson cascade is treated in detail, taking into account energy loss and decay in an atmosphere of varying density. All the energy of the collision is assumed to be radiated as pions, with values for longitudinal and transverse momenta based on the results of emulsion experiments.

Holyoak et al (1966) have used the C.K.P. Model and a diffusion equation describing the pion cascades from individual interactions of the leading particle. The diffusion equation is solved using the method of successive generations, simplifying the calculations by neglecting the effect of the decay of pions on the longitudinal distribution of their interactions in a given generation. The total number of electrons is calculated using solutions of the cascade equations under Approximation B, and a Monte-Carlo method.

Calculations have also been made by Dedenko (1966), which employ methods similar to those of Hillas (1966), avoiding the method of successive generations for the solution of the diffusion equations.

In general, the theoretical models are able to describe some of the main features of EAS, but are unable to give any detailed predictions, owing to the number of unknown parameters involved in the processes of high-energy nuclear interactions.

1-1.4 The Muon Component

Muons in EAS are characterised by their ability to pass through large quantities of absorber without interacting, and, although they are 50 to 100 times less dense than the electrons near the centre of the shower, they are found in large numbers at large distances from the core. The muon component carries a high percentage of the primary energy, many times that of the electron-photon component, and the lateral distribution as a function of energy provides an immediate indication of the transverse momentum and abundance of the parent pions. Unlike the nuclear-active and electromagnetic components, the muons are only slightly depleted in traversing the atmosphere, and indeed, only 30% are lost through decay and ionization. The ratio of positive to negative muons in EAS indicates the nature of the parent particles produced at these high energies.

The comparative ease of detection of the muon component in comparison with the nuclear-active component, and its closer relationship with the primary interaction than the electromagnetic component, has led to an increasing interest in its properties. Some of the previous experiments designed to measure the energy spectrum of muons in EAS will be summarised in the next section.

1-2 Previous Experiments on the Muon Component in EAS.

The momentum spectrum of muons in large EAS is not well known, and previous experiments have yielded conflicting results. The

majority of these determinations have been absorption experiments, generally in the regions of shower size 10^4 to 10^5 particles. The results of the absorption experiments of Dovzhenko et al (1957), Andronikashvili et al (1960), and Vernov et al (1960) are shown in fig.1.1, in the form of integral spectra, with the distant spectra normalised at 2 GeV/c.

Bennett and Greisen (1961) used a magnet spectrograph to determine the spectra of muons in showers in the range 10^4 to 10^7 particles, at lateral distances from 25 to 475m. The number of particles detected was limited by the small collecting power of the instrument, and individual determinations of core distances and shower size were not made. The integral spectra found in the experiment are shown in fig.1.2, together with curves corresponding to the empirical relation suggested by Greisen as a representation of the experimental data; namely,

$$\rho_\mu(\geq E,r,N) = \frac{14{\cdot}4r^{-0{\cdot}75}}{\left(1+\frac{r}{320}\right)^{2{\cdot}5}}\left(\frac{N}{10^6}\right)^{0{\cdot}75}\left(\frac{51}{E+50}\right)\left(\frac{3}{E+2}\right)^{0{\cdot}14r^{0{\cdot}37}}$$

De Beer (1962) derived a muon momentum spectrum from a scattering experiment using spark chambers and absorber. The integral spectra given by de Beer are shown in fig.1.2.

1-3 The Present Experiment

The experiment is designed to measure the momentum spectrum in the momentum range1to 100 GeV/c in EAS of size 10^5 to 10^8

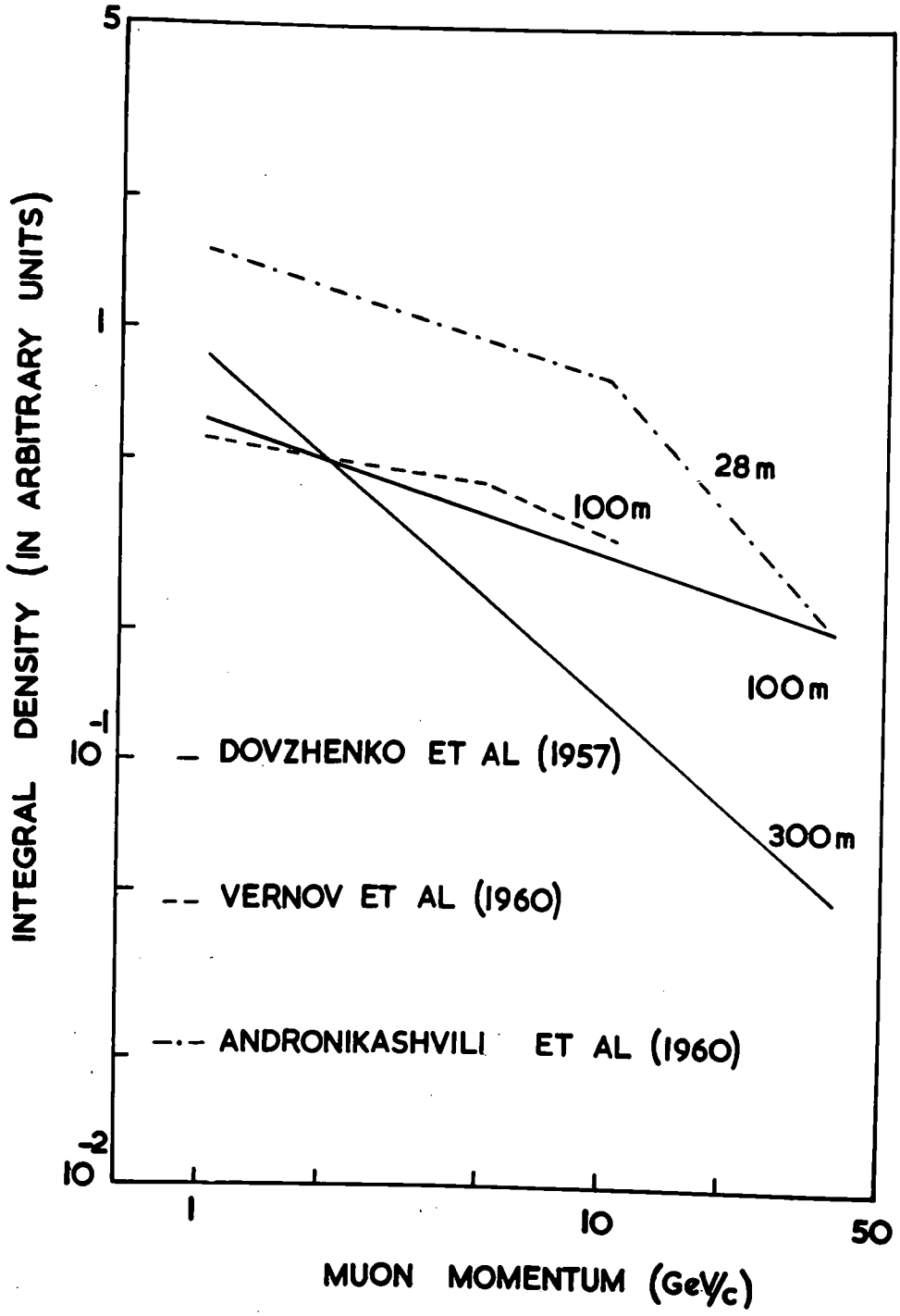
INTEGRAL DENSITY (IN ARBITRARY UNITS)
5
1
10⁻¹
10⁻²
28m
100m
100m
300m
— DOVZHENKO ET AL (1957)
-- VERNOV ET AL (1960)
-·- ANDRONIKASHVILI ET AL (1960)
1
10
50
MUON MOMENTUM (GeV/c)

FIG. 1.1

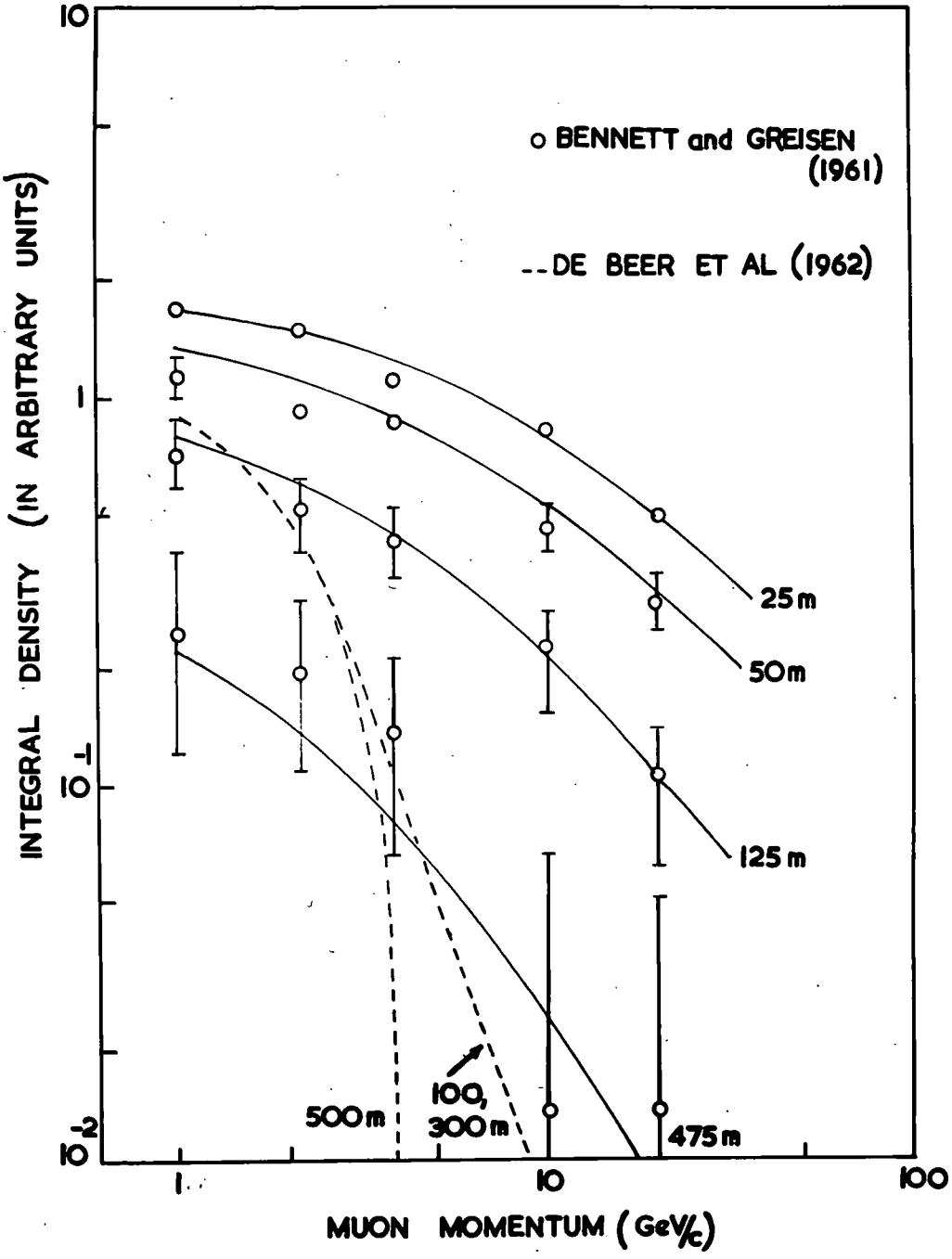
10
1
10⁻¹
10⁻²
INTEGRAL DENSITY (IN ARBITRARY UNITS)
o BENNETT and GREISEN (1961)
--DE BEER ET AL (1962)
25m
50m
125m
475m
500m
100, 300m
1
10
100
MUON MOMENTUM (GeV/c)

FIG. 1.2

particles, at lateral distances from the shower core ranging from 10 to 600m. It comprises a magnet spectrograph located at the centre of three EAS arrays (fig.3.1), each detecting showers in a narrow band of sizes. The arrays are capable of locating the core position for each detected shower, so allowing the size to be estimated, and of giving information on the arrival directions of showers. Consequently, the data may be subdivided into intervals of shower size, lateral distance, and arrival direction.

CHAPTER 2

THE HAVERAH PARK SOLID IRON MAGNET SPECTROGRAPH

2-1 Introduction

The design of a cosmic ray spectograph is often the result of a compromise between a requirement for a large collecting power and a high maximum detectable momentum (m.d.m.). Because of this limitation, two types of spectrograph have been evolved: those designed to measure the momentum spectrum and charge ratios of single unassociated muons and those instruments designed to investigate muons in extensive air showers (EAS). The high rate of single muons enables an investigator to use a spectrograph having a relatively small collecting power (defined as $\iint dA.\, d\omega$, where dA is a small element of sensitive area, and $d\omega$ its opening angle) which is a consequence of the large separation of the detecting layers necessary for a high m.d.m.

A spectrograph for use in conjunction with an EAS array requires a modification in the design to allow for the small intensity of EAS of a particular size which are incident on or near the instrument in a given time, and which are distributed over a large range of arrival directions. So that full use may be made of all detected showers, a large collecting power is necessary, and consequently a modest m.d.m. must be tolerated. Investigations of the momentum range 1 to 100 GeV/c, which are of considerable interest in EAS studies, can be made using the spectrograph described in this chapter.

2-2 Previous Magnet Spectrographs

Early experimental determinations of the momentum spectrum of unassociated muons were made using air-gap magnets employing Geiger-Muller (GM) detectors. (Hyams et al (1950), Owen and Wilson (1955)). The advantages of the large sensitive areas available from the use of GM detectors were offset by their poor spatial resolution, and the GM counters were replaced as track locators by cloud chambers (Holmes et al (1961), Pine et al (1959)). The difficulties encountered in the operation of large size cloud chambers imposed a limit on the collecting power and considerably reduced the reliability of such types of spectrograph.

Table 2.1 summarises briefly the properties of some of the most recent cosmic ray spectrographs. The introduction of neon flash tubes considerably increased the collecting power of these spectrographs since large areas could be covered with a detector of high spatial resolution and moderate cost. The spectrograph of Pine et al was modified (Roe et al (1959)) by the replacement of the cloud chambers with neon flash tubes. Small flash-tube spectrographs were also operated by Coates (1961), and Ashton et al (1959), and the Durham vertical spectrograph, using geiger counter detectors (Brooke et al (1962)), was improved by the addition of flash tubes, as described by Hayman and Wolfendale (1962).

The limiting factor in the accumulation of data at high momenta is the small magnetic field volume produced by air-gap magnets

Authors	Solid iron/ Air gap	Detectors	m.d.m.	
Brooke et al (1962)) Jones et al (1962))	air gap	GM	26.5	
Hayman and Wolfendale (1962)	air gap	GM/FT	660	
O'Connor and Wolfendale (1960)	solid iron	GM	10	
Ashton et al (1963)	solid iron	GM	40	horizontal C.R.
Ashton and Wolfendale (1963)	solid iron	GM/FT	179	
Bull et al (1965)	solid iron	FT	360	
Bennett and Greisen (1961)	air gap	GM	20	EAS work
Present experiment	solid iron	FT	60	

Table 2-1

with a moderate power dissipation. Solid iron magnets have the advantage of an increased field and magnetic volume for the same expenditure of energy, and also the magnetic material acts as an absorber of known thickness eliminating all but the hard component. Preliminary investigations by Bennett and Nash (1960) on the properties of solid-iron magnets led to the large spectrograph at Nottingham (Bull et al (1965)), and the spectrograph at Durham (Ashton et al (1963), Ashton and Wolfendale (1963)).

The only previous spectrograph measurements on the momentum spectrum and charge ratio of muons in EAS were made by Bennett and Greisen (1961), using an air-gap magnet - Geiger counter spectrograph with an m.d.m. of 20 GeV/c. The magnetic field of 12 kgauss extended over an area of $0{\cdot}6 m^2$, and a depth of 20cm. For track location, three trays of $\frac{5}{8}$" GM counters were spaced above, below and within the magnet gap. The spectrograph aperture was $25{\cdot}4\ cm^2$-sr for undeflected particles, but was reduced by 33% by counter layer inefficiencies.

2-3 The Haverah Park Spectrograph

The Haverah Park spectrograph comprises a large solid-iron magnet and neon flash tube trays for accurate track location. The size and disposition of the magnet and flash tube trays is shown in fig.2.1. The four 'momentum trays', containing seven layers of tubes, are of two sizes: the extreme trays (A1 and B1) each have 120 tubes per layer, and the inner trays (A3 and B3) 103 tubes. The 'direction trays'(A2 and B2) have four layers, each of 98 tubes.

HAVERAH PARK SPECTROGRAPH

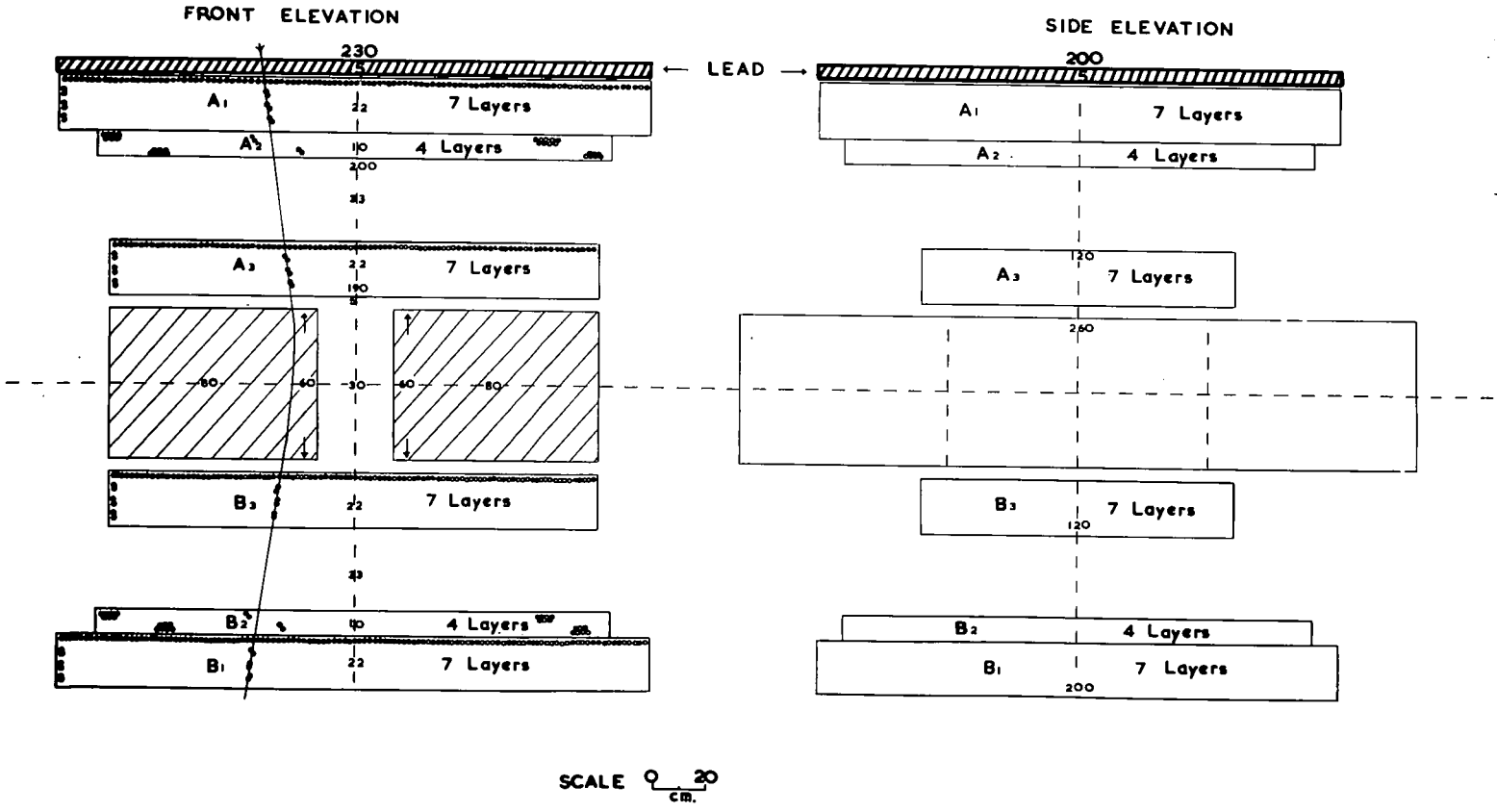

FIG. 2.1

The total sensitive area of the magnet is $1 \cdot 8 m^2$ for a particle incident from the vertical direction, and the opening angle is approximately 1 steradian. The aperture of the instrument for an undeflected particle is $1 \cdot 1$ m^2-sr. A uniform induction of 14·6 kgauss gives an m.d.m., defined by the standard deviation of the noise distribution of the instrument, of 60 GeV/c for a vertically incident particle.

2-4 The Magnet

2-4.1 Specification

The magnet is of the type developed by the Durham and Nottingham groups (O'Connor and Wolfendale (1960), Bennett and Nash (1960)). The plan of the magnet (fig.2.2) is a rectangular picture-frame, the inside corners of which are rounded to extend the useful region of induction. The composition by weight of the steel used has been given by Bennett and Nash (1960). It is important that steel with a low carbon content is used to reduce the coercive force, and hence the field required to saturate the magnet. The magnet is 60cm thick (472 gm cm^{-2}), composed of 45 half-inch plates, with 1 one-inch base-plate for mechanical support.

The choice of thickness of the magnet is governed by three factors: the minimum detectable momentum, the ratio of the magnetic deflection to the root mean scattering deflection, and the maximum detectable momentum. For the Haverah Park Magnet, the minimum detectable momentum is 0·9 GeV/c, the ratio $\Delta\psi_m / \Delta\psi_s \simeq 3$, where

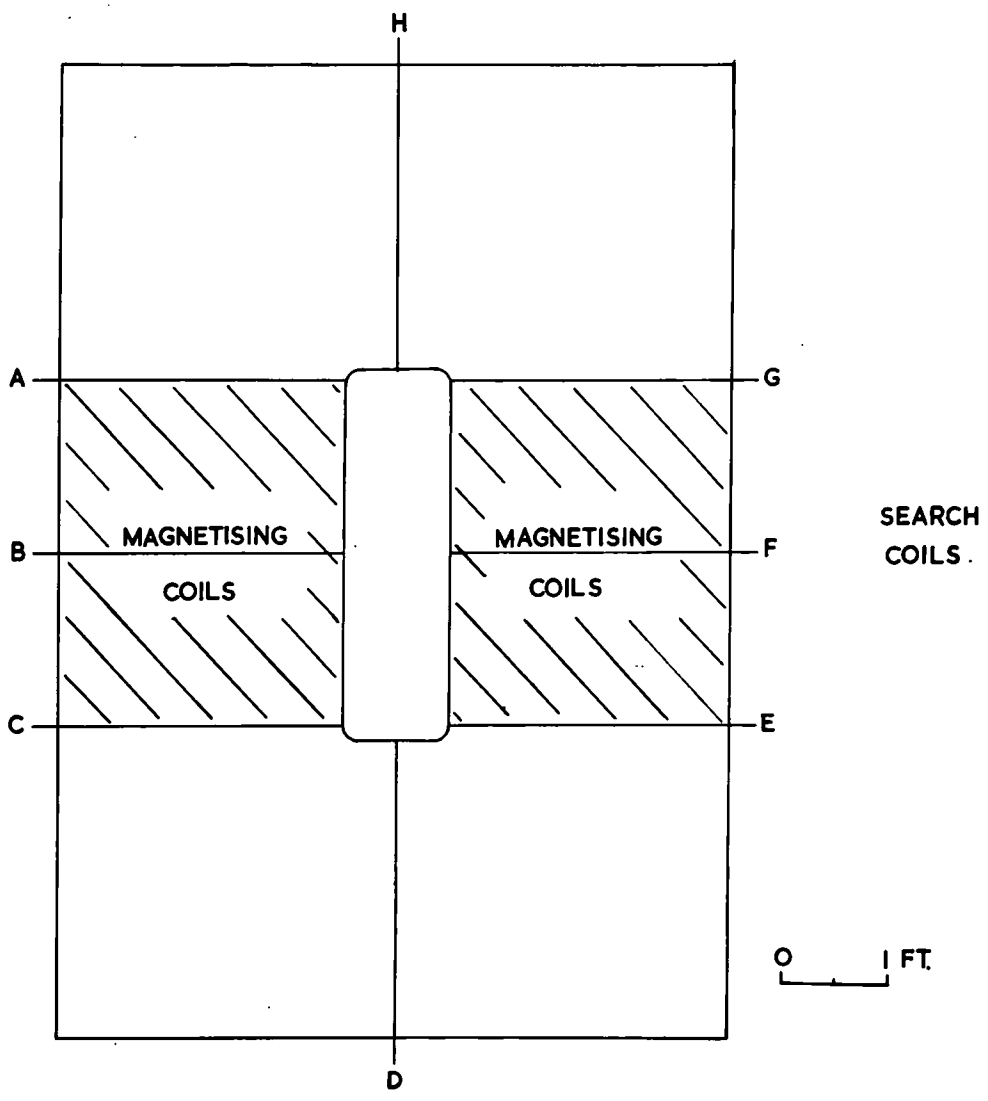
H
A
G
B
F
C
E
D
MAGNETISING
COILS
MAGNETISING
COILS
SEARCH
COILS.
O
I FT.

FIG. 22

$\Delta\psi_m$ and $\Delta\psi_s$ are the deflections due to the magnetic field and the scattering in the magnet material respectively, and the m.d.m for a vertical particle, defined by $\Delta\psi_m$ = the 'noise', is 60 GeV/c. The 'noise' has been found by the quadratic addition of the standard deviations of the distributions of the scattering and measuring errors.

Three hundred and twenty five turns of double cotton covered, enamelled, 14 gauge copper wire are wound on each arm of the magnet, and series connected. The total resistance of the coils is 10·7 ohms, and they dissipate 2·3kW for an energising current of 14 amps. This power raises the temperature of the magnet to 31°C and the energising coils to 37°C.

2-4.2 Field Measurements

Search coils of lumex covered 22 SWG wire enclosing different sections of the magnet have been inserted at positions round the magnet circumference as shown in fig.2.2. Measurements of the field have been made by connecting a calibrated fluxmeter to each of these search coils in turn and reversing the energising current. Fig. 2.3 shows the variation of the observed induction with the number of plates enclosed for both arms of the magnet (positions F and B). The variations of the measured induction with depth through the magnet can probably be ascribed to the variation in the thickness and width of the laminations, since these errors are of the same size, 3%, as the variation in induction. The mean of the readings for the largest search coils, which enclose the total magnet cross-section, yields a

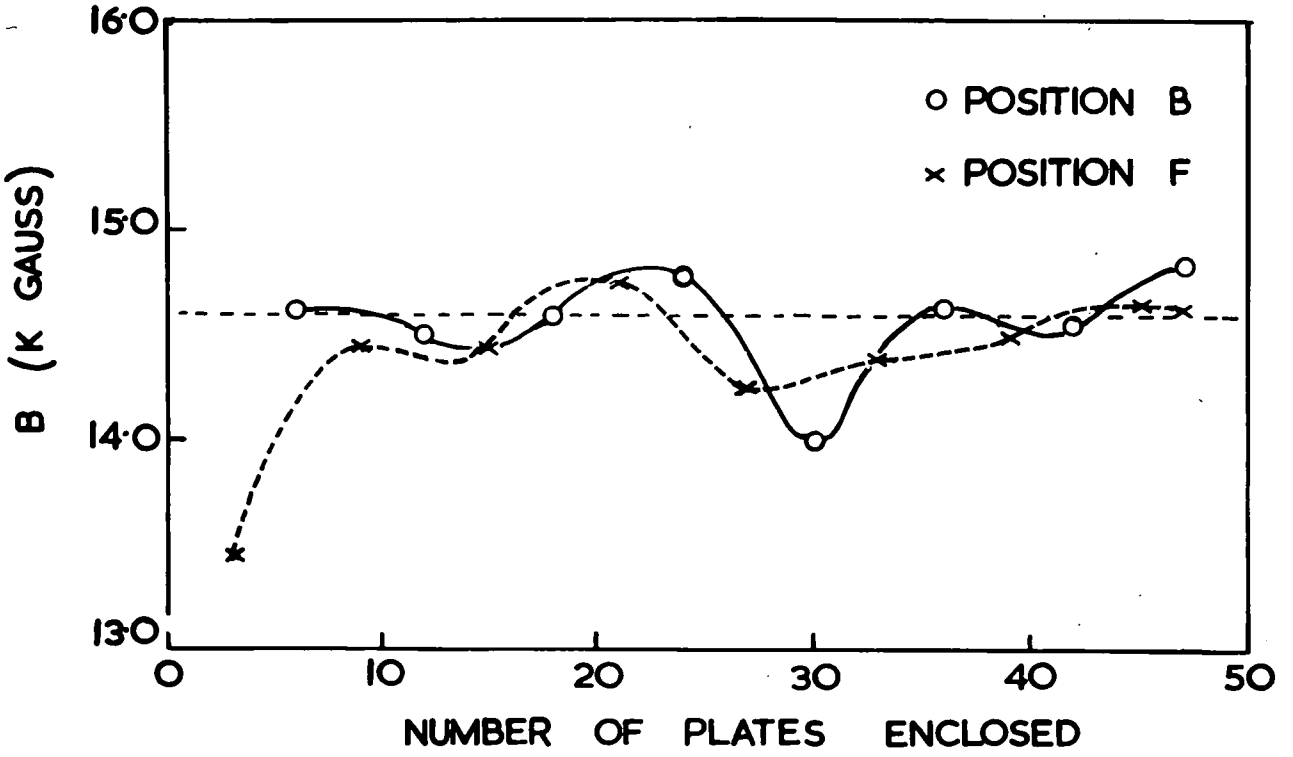
16·0
15·0
14·0
13·0
B (K GAUSS)
o POSITION B
× POSITION F
0
10
20
30
40
50
NUMBER OF PLATES ENCLOSED

FIG. 2.3

value of 14·6 ± 0·3 Kgauss.

2-5 The Visual Detectors

2-5.1 Choice of Detectors

Several types of detector, visual and non-visual, are suitable for use in spectrographs. Most early workers (Caro et al (1951), Owen and Wilson (1955), Bennett and Greisen (1961)) used geiger counters arranged in layers above and below the magnet, and in some cases between the magnet poles. A more accurate technique of track location, cloud chambers, necessitated a large reduction in collecting power, and the maximum detectable momentum was limited by track distortion. Greater accuracy was achieved using spark chambers (Alkofer (1960)) and flash tubes (Ashton et al (1959)). Since the difficulty of operating large spark chambers was considered to outweigh the advantage of their greater resolution, flash tubes were selected for the present experiment.

The neon flash tube was first introduced by Conversi and Gozzini (1955). Further improvements were made by Barsanti et al (1956), and the Durham workers (Gardener et al (1957)), resulting in the 'EAS tubes' (Coxell and Wolfendale (1960)) used in the present experiment. The internal diameter of the 'EAS tubes' is 1·6cm, and is the result of a compromise between the requirements of the accuracy of track location, and the large time delay, 20 microseconds, needed for other air-shower apparatus in the vicinity to complete its recording before the EHT pulse is applied to the tubes. To maintain

the efficiency with a large time-delay, the ions along the particle track require a large mean distance to travel to the tube walls, so that attachment losses are minimised.

2-5.2 Summary of the Properties of the Flash Tubes used in Air-Shower Work

A full description of 'EAS tubes' is given by Coxell and Wolfendale (1960) and hence reference will only be made here to the variation of efficiency of the tubes (that is, the probability of a tube discharging when traversed by a particle) as a function of the pulse height, the time-delay between the arrival of the particle and the application of the pulse, and the rise time of the applied pulse. The results of efficiency versus time-delay and pulse height are shown in fig. 2.4. It is found that the value of rise time of the applied pulse is not very critical. The mechanical specification of the tubes is given in table 2.2.

2-5.3 Design of the Flash-Tube Trays

The main requirement of the trays is that they provide a rigid and accurate support for the tubes in a configuration designed so that the maximum number of tubes is traversed by particles having arrival directions up to 30° from the vertical. To minimise the thickness of the flash-tube trays, the tubes are mounted in one single and three double layers. The optimum arrangement for the layers is found using an analogue method in which scale drawings are made of each layer of tubes, and then adjusted to give the best value of the

Glass	Soda (GEC X 8)
Internal diameter	1·6 cm
External diameter	1·8 cm
Length Tray A1, B1	200 cm
A3, B3	120 cm
Straightness	1 mm in 120 cm
Gas pressure	60 ± 1 cm Hg.
Gas content	98% Ne, 2% He, 10^{-4}% air
Painting	first 20cm of tube white, total tube painted black.

Table 2-2

response of the tray for particles incident between 0° and 30° from the zenith. The tubes are supported at each end by 0·6" square-section dural tubes. The lower layers of tubes are located in accurately milled slots in these supports, as shown in fig.2.5, and are in turn used to locate the upper layers.

The electrodes are 24 gauge aluminium sheets, inserted above and below each double layer, and bound at the edges with insulating material to eliminate discharging and sparking. In order to identify the trays on the film, small fiducial lights are attached to each end and illuminated for every exposure. In addition, to reduce the contamination from the electrons in showers falling with their axes close to the spectrograph, 5 cms. of lead has been placed above tray A1.

2-5.4 The Direction Trays

Many events occur where two or more muons pass through the apparatus with very small projected lateral separations. After the particles have undergone magnetic deflection and Coulomb scattering the correlation of the top and bottom half-tracks is often difficult. So that these events are not wasted, two further trays of flash-tubes (A2 and B2) have been introduced. (see fig.2.1). These trays each contain two double layers of tubes, mounted in the same manner as the four momentum-measuring trays. Distances of particles in the back-front direction of the instrument are then estimated by offsetting each double layer in the direction trays at a small angle ($3\frac{1}{2}^{\circ}$) in

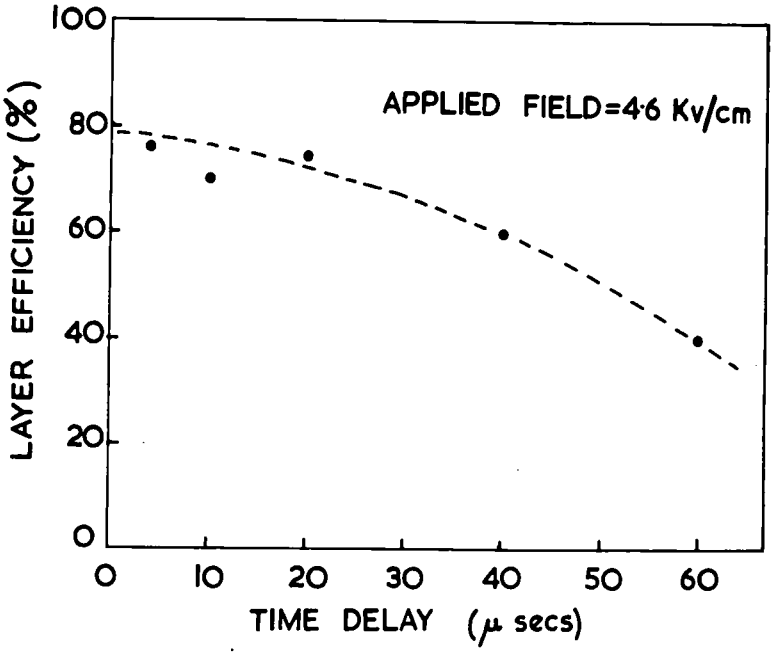
100
80
60
40
20
0
LAYER EFFICIENCY (%)
APPLIED FIELD=4·6 Kv/cm
0
10
20
30
40
50
60
TIME DELAY (μ secs)

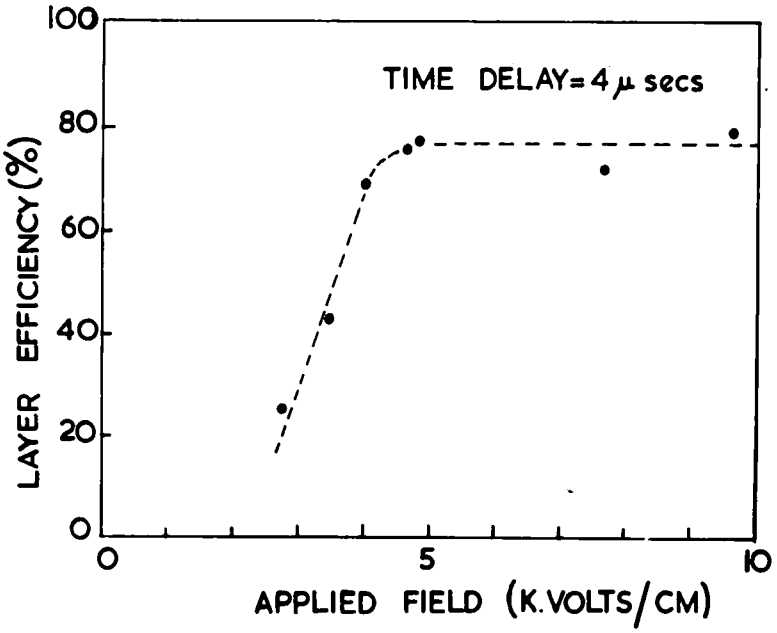
100
80
60
40
20
0
LAYER EFFICIENCY (%)
TIME DELAY= 4 μ secs
0
5
10
APPLIED FIELD (K.VOLTS/CM)

FIG. 2.4

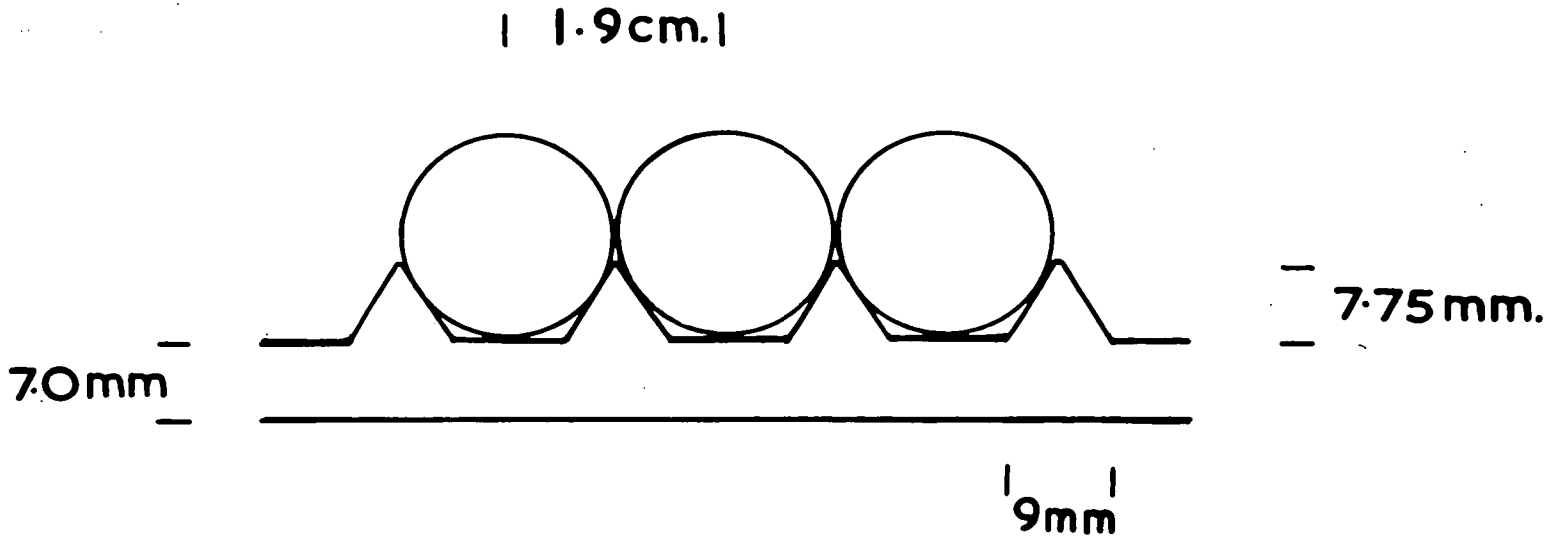

FIG. 2.5

opposite directions. The angular displacement is required to be small to exclude the possibility of ambiguity between particles, since tubes set at a larger angle would give several possible positions for each particle. Accuracy of location in the back-front direction using these trays is between 3 and 12 cms., depending upon the number of tubes traversed. In practice, it is found that correlation between the half-tracks in high density events, by comparison of the relative depths of the particles, is still difficult, and lower density events generally do not require this technique. Consequently, the method has proved of only limited use.

2-5.5 The Photography

Owing to the very narrow polar angle of the light emitted by the flash tubes (Coxell and Wolfendale (1960)), it is necessary to view the eight feet wide trays of the spectrograph from a large distance. Maximum use is made of the working space available by employing the mirror system shown in fig.2.6. The periscope system enables all flash tubes to be photographed in a single 35mm frame by omitting the magnet from the field of view of the camera. Because of the small size of the flash tube images (120 microns) it would be difficult to ensure correct identification of flash tubes unless mirrors of high quality are used. Back-silvered "float-glass" mirrors have been found to be quite satisfactory. The camera is a Shackman model AC2/25, equipped with a high quality f1.8, 10cm focal length lens. The film must be fast; most data have been recorded on Ilford HPS film.

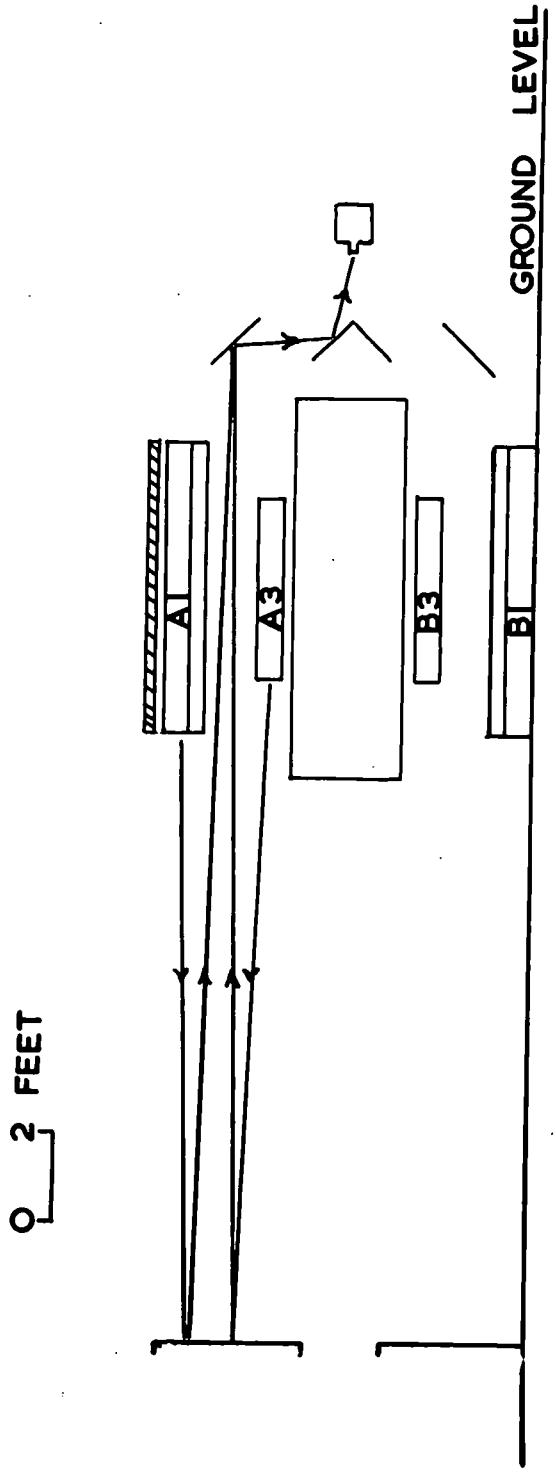

FIG. 2.6

2-5.6 The Accurate Measurement of the Flash Tube Positions

An accurate determination of the deflection of a particle depends upon the accurate alignment of the tubes and the measurement of their positions. To this end, the spectrograph is provided with eight plumb lines, defining two parallel planes at either side of the magnet, which may be viewed by telescopes mounted on two rigid vertical beams at a distance of 10 feet from the spectrograph. In this way, it is possible to check that no movement of the spectrograph occurs during the period of operation. The same plumb-lines form a plane of reference for the alignment and measurement of the neon flash tubes. Horizontal measurements have been carried out using a travelling microscope, or, for extremely long traverses, an optical bench carrying a telescope. The optical bench is used in conjunction with a good metre rule, which is placed alongside the tubes to be measured. Vertical measurements have been made using a cathetometer or a travelling microscope. Table 2.3 contains a summary of the measurements, and their estimated errors.

The angular error resulting from the measurement is almost entirely due to the horizontal error, since the vertical distance between trays is large compared with the errors involved. For this reason, the tubes are mounted so that their curvature (if any) is contained in a vertical plane.

	Position (mm)		Mean	Mean
	Vertical	Horizontal	Inclination(mm)	Skew(mm)
A1	2076•6 ± 0•1	26•2 ± 0•3	+ 0•4	- 0•35
A3	1437•2 ± 0•1	147•5 ± 0•3	+ 0•5	+ 0•1
B3	560•6 ± 0•1	150•9 ± 0•3	- 0•2	+ 0•25
B1	0	29•0 ± 0•3	+ 0•2	+ 0•1

Mean distance between adjacent tubes = 19•070 ± 0•002 mm

Maximum skew of a layer of tubes = 9'

Maximum inclination of a layer of tubes = 30'

Mean distance between adjacent layers = 46•10 ± 0•04 mm

Table 2-3

2-6 The Acceptance Function of the Spectrograph

2-6.1 The Need for a Knowledge of the Acceptance Function

For a determination of the momentum spectrum of the muons incident on the spectrograph, the probability of acceptance by the spectrograph of particles of all momenta, incident and emergent at all angles, must be known. The variation of the probability of acceptance of a particle by the spectrograph (hereafter called the acceptance function) is due to the following:-

a) The wide distribution of arrival directions of the muons.

b) The different signs of the charge of the muons.

c) The different momenta of the muons.

d) The absorption of muons by the magnet.

The correction for the variation of the acceptance function with the sign and with the absorption of particles at low energies is necessary for all methods of analysis of the data. The two methods of analysis employed in the present experiment, however, require the acceptance function to be expressed in different forms.

2-6.2 The Acceptance as a Function of the Incident Angle and Deflection

The acceptance as a function of the incident angle, ψ_0 and the deflection, $\Delta\psi$ has been evaluated by an analogue method. A scale drawing of the spectrograph is prepared showing the sizes and positions of the magnet and flash-tube trays. A protractor is then used to determine the extreme limits of the sensitive area for various incident and emergent angles. From this, the sensitive area for a particle with incident angle ψ_0 and deflection $\Delta\psi$ is calculated and expressed as

a fraction of the sensitive area presented to a vertical particle of infinite momentum. The acceptance function is shown in fig 2.7.

2-6.3 The Acceptance as a Function of Momentum and Incident Angle

The dependence of the acceptance function on the momentum and incident angle of a muon has been found by an analytical method. For several values of incident angle, and with values of momentum extending across the useful momentum range of the spectrograph, the deflection and horizontal displacement of a particle from the point of incidence at the top of the magnet is calculated. From the dimensions of the magnet and tray B3, and their separation, the sensitive area of B3 available to all combinations of momentum and incident angle are evaluated. This area is then compared with the sensitive area presented to a vertical particle of infinite momentum. The effects of the absorption of low energy particles by the magnet is then taken into account, imposing a cut-off at high angles of incidence. Except for small differences at low momenta (or high deflections), the two acceptance functions are identical.

2-7 Interpretation of the Photographic Records

2-7.1 The Multiple Exposure using a Radioactive Source

Using a 3 mc. Co^{60} radioactive source, and repeatedly pulsing the flash tubes, an exposure has been made showing the location of every tube. Copies of the reprojected image of the exposure are used to locate and draw out the muon trajectories. One of these diagrams is shown in fig. 2.8, where the crosses indicate the position

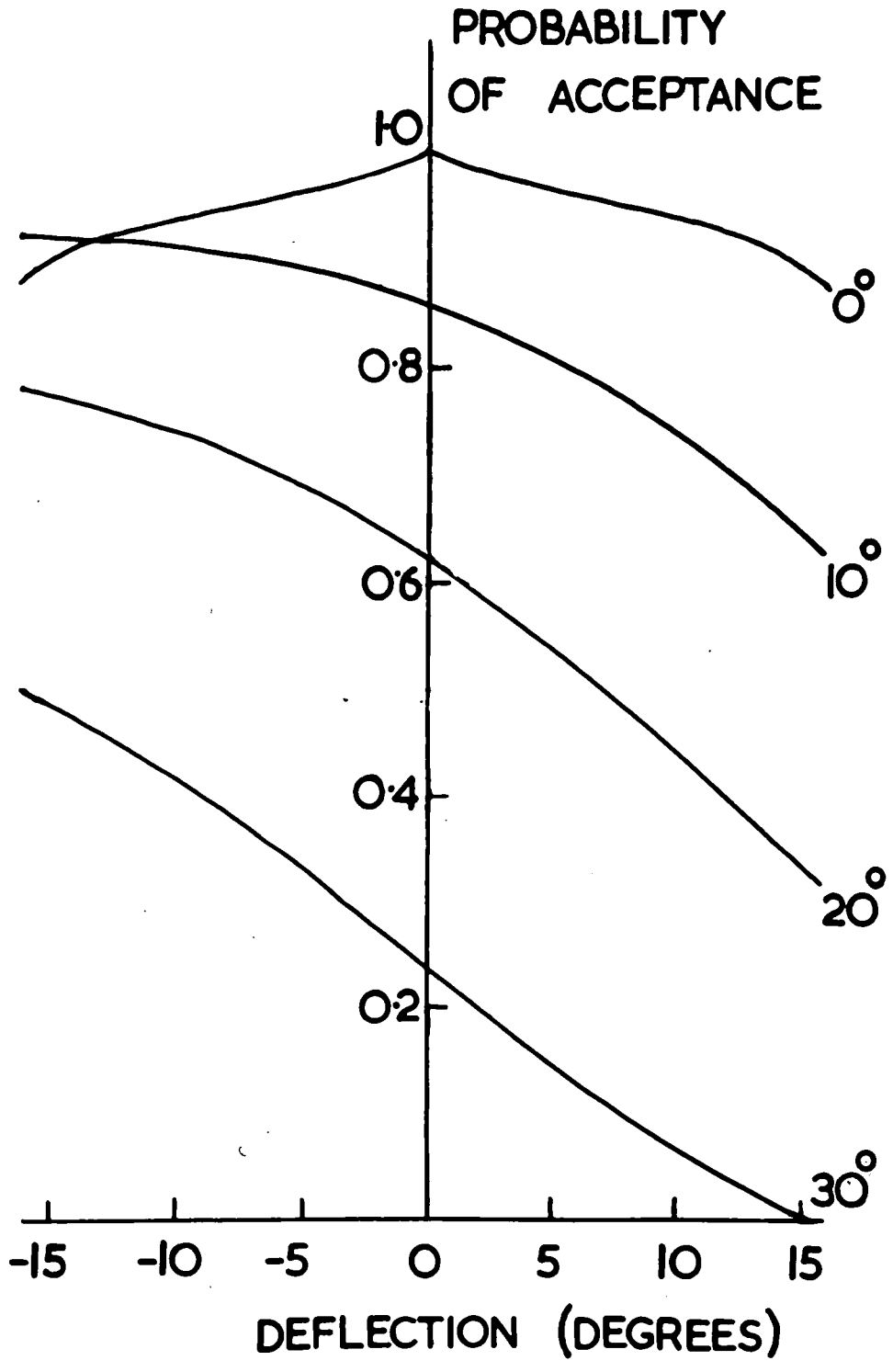
PROBABILITY
OF ACCEPTANCE
1·0
0·8
0·6
0·4
0·2
0°
10°
20°
30°
-15
-10
-5
0
5
10
15
DEFLECTION (DEGREES)

FIG. 2.7

of the fiducial lights on each tray. The cross-section of the magnet is reinserted in the drawings so that particles passing through the central hole, or emerging from the sides of the magnet are quickly rejected. An accurate check that all particles have traversed the magnet fully is made at a later stage.

2-7.2 The Simulation of a Particle Trajectory

The track simulator, shown in fig. 2.9 with part of the event from fig. 2.8 displayed, is an 8/10 scale diagram of the flash tube trays. The circles represent the mean inside diameter of the flash tubes, found from a series of measurements on randomly selected (broken) flash tubes. The muon track is represented by a scribed line on a transparent rule, and the best track is estimated from the knowledge of the probability of the flashing, or non-flashing, of the tubes as a function of the position of the track in them. It is expected in the near future to replace the manual simulation by a computer programme based on the same technique of the summation of probabilities. The estimated accuracy of track location in each half-track on the simulator is $0{\cdot}2^{\circ}$, giving an accuracy of $0{\cdot}3^{\circ}$ for the measured particle deflection. The expected accuracy from the computer analysis of the track-fitting is the same, the major advantage being the considerable reduction in the labour of simulation.

The Durham Elliot 803 computer has also been programmed to accept the simulated tracks and calculate the position of the intersection of the extrapolated tracks inside the magnet. Possible particle trajectories with intersections lying outside the magnet volume are

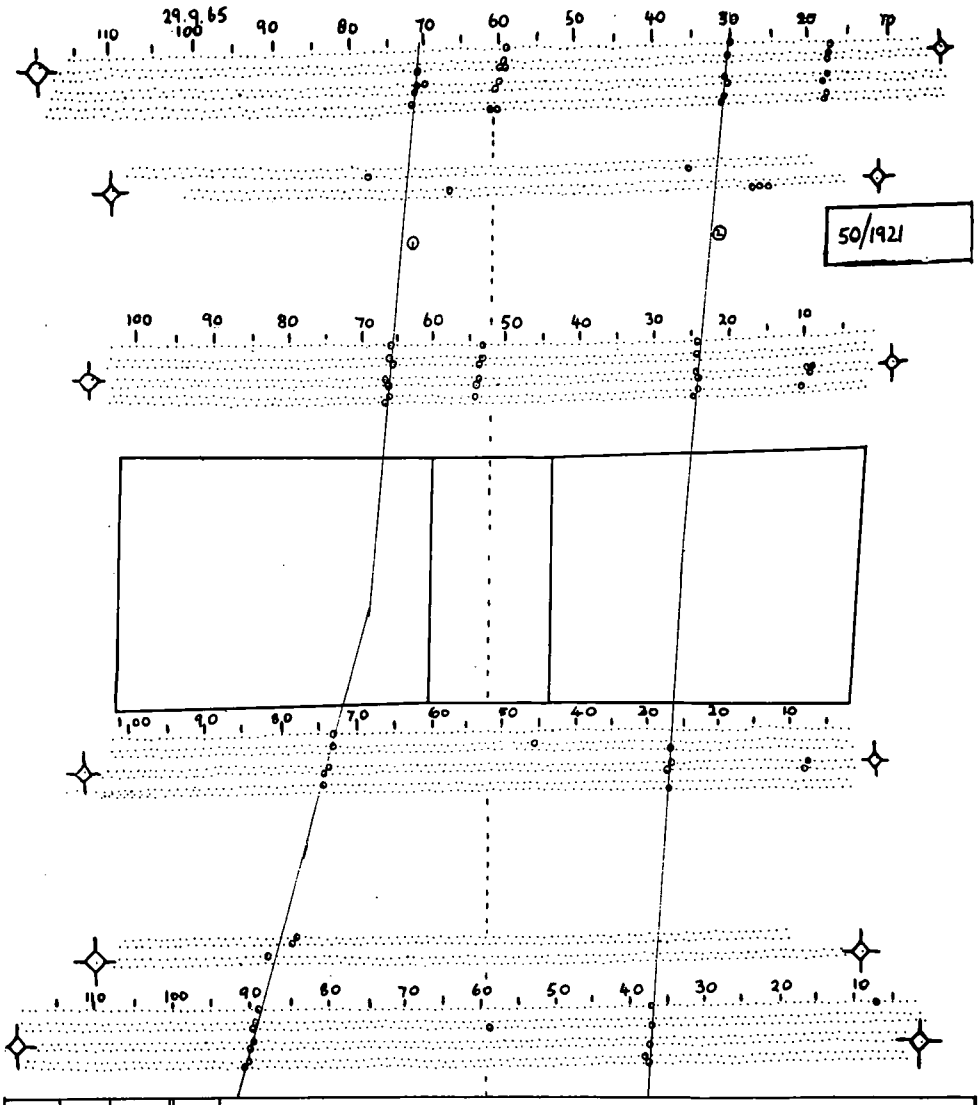

F188		50		1		2									
		3.5×10^5		A	B	A	B								
H⁻		/	P	9·0	2·5	2·8	11·1								
		/	Q	12·0	8·9	4·75	12·6								
032697		54m	N'	20	3	10	17								
	X	+21m													
	Y	-69m													

FIG. 2.8

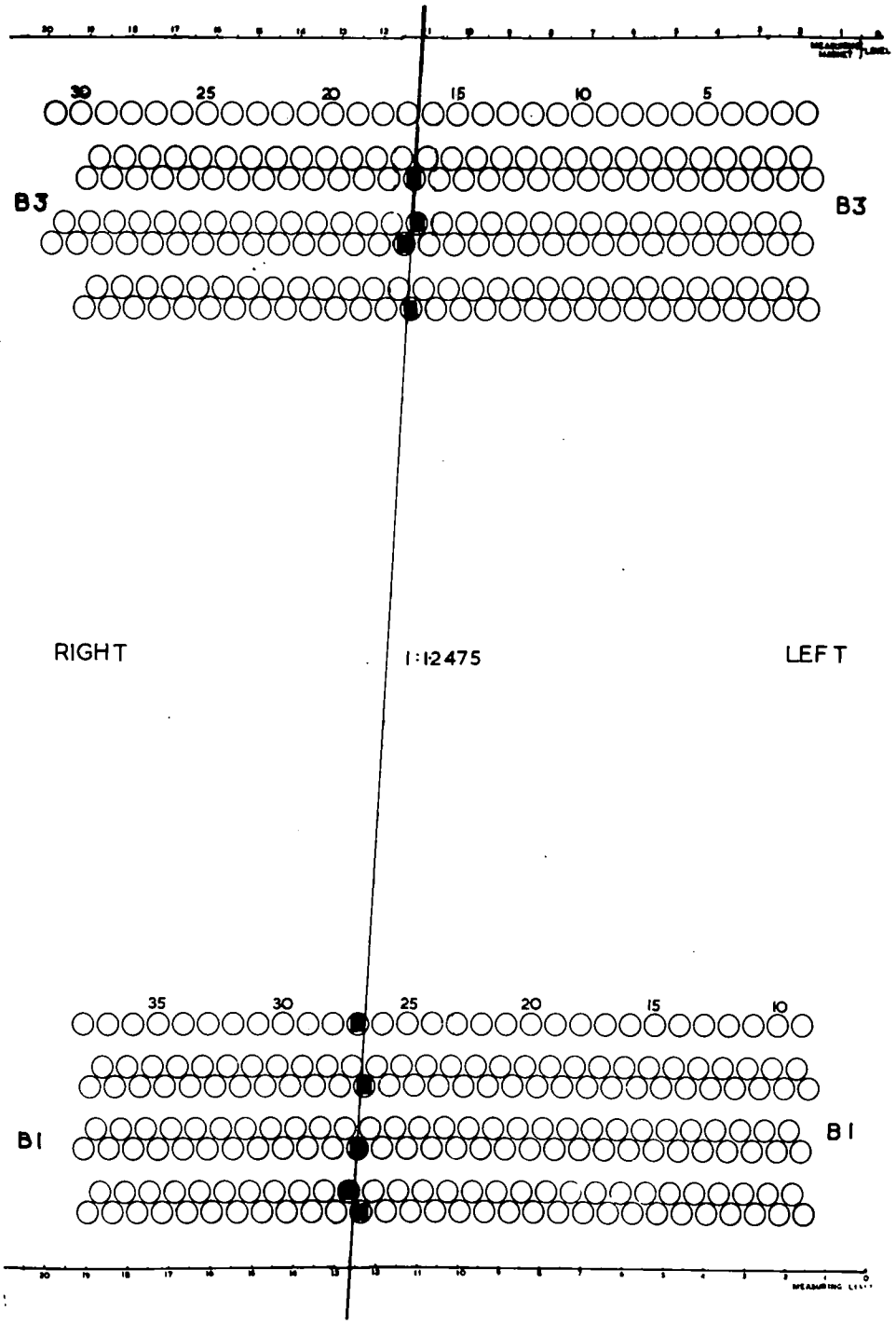

FIG. 2.9

rejected, as are the tracks of muons emerging from the sides of the magnet. The computer determines the deflection of the particle, the sign of the charge (dependent on the arm of the magnet traversed, and the field polarity), and tabulates this and related data for each event. The events are then classified according to usefulness, combined with their EAS data, and are summarised on punched tape for further computation. The criteria used in selecting useful events are:-

a) There should be no possibility of confusion between neighbouring tracks.

b) The particle must have passed through fewer than two non-flashed tubes.

c) The particle trajectory should have the same incident direction as the rest of the shower particles, to eliminate chance unassociated events, which are found to occur with a relative frequency of about 0·2%.

2-8 Investigation of the Noise of the Instrument

At momenta above the m.d.m., the width of the track fitting error distribution, δ_{exp}, is large compared with the deflections due to the magnetic field. To ensure that the correct muon momentum spectrum is deduced, exhaustive tests to determine δ_{exp} have been conducted, all of which are consistent with the value of $0{\cdot}3^{o}$.

2-8.1 Determination of the Noise from Muons which have Traversed the Central Hole of the Magnet

The measured deflection of muons which have traversed the central hole of the magnet and reached the standards required for

useful events, given in section 2-7, are plotted (fig.2.10) and the standard deviation of the distribution found. The curve in fig.2.10 is the Gaussian of equal area and standard deviation from the mean of 18 minutes, which is by definition, the noise of the instrument.

2-8.2 Estimate of the Track-Fitting error

An estimate of the angular error of the track-fitting procedure has been made from trials of the accuracy to which a muon trajectory can be reconstructed on the simulator. An accuracy of $\pm$ 0·075 inches at each of the measuring levels shown in fig.2.9, is taken as the best estimate. The measuring levels are twenty-eight inches apart, and an angular accuracy of $\pm$ 0·2° for each half-track is found from the quadratic addition of the contributions from both levels. The process is identical for the second half-track, and the accuracy of the determination of the deviation of a muon through the magnet, given by the contributions from both half-tracks added quadratically, is 17 minutes.

2-8.3 The Distribution of the Distances between the Projected Half-Tracks at the Centre-Level of the Magnet

The computer programme used to determine the point of intersection of the projected half-tracks, described in section 2-7.2, also computes the distance, Δy_m, between the extrapolated half-tracks at the centre level of the magnet. To minimise the effects of scattering in the magnet, all events with a deflection greater than 1°, equivalent to a momentum of 15 GeV/c, have been rejected, and the

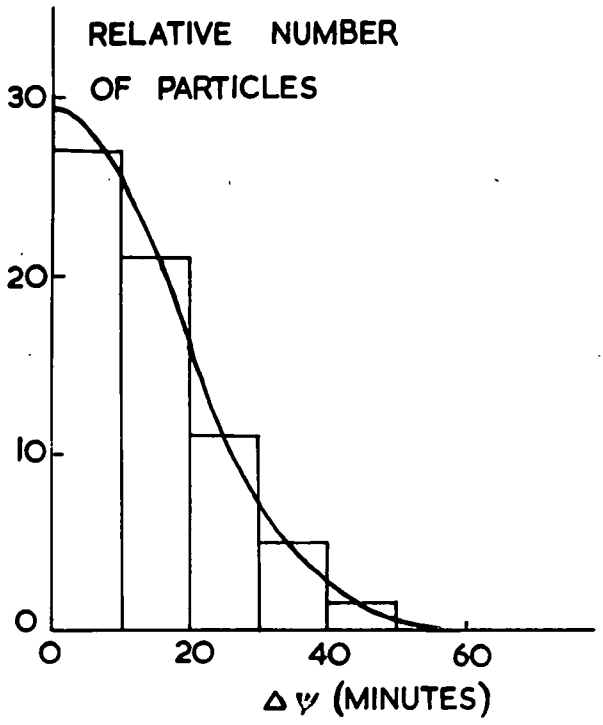

FIG. 2.10

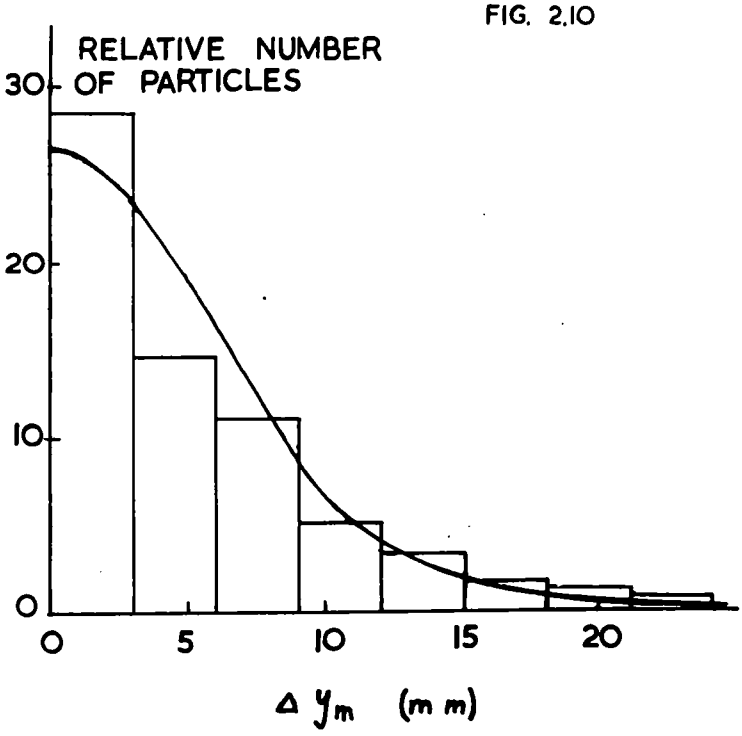

FIG. 2.11

distribution of the values of Δy_m plotted for the remaining particles. The distribution is shown in fig.2.11, with a Gaussian distribution of equal area and a standard deviation of 6mm superimposed. The standard deviation represents the contributions from both half-tracks, which are equal, and have a value of 4mm. The distance between the centre level of the magnet and the level equidistant between the flash tube trays in each arm is 650mm. The angular error for each half-track is therefore $0{\cdot}35^{\circ}$, and the error on the measurement of the deflection of a muon is $0{\cdot}49^{\circ}$, or 29 minutes. This is an upper limit to the value of the error, since it also includes the Coulomb scattering of muons in the magnet, which may be as large as $0{\cdot}3^{\circ}$ for the selected particles.

2-8.4 The Zero-Field Run

Upon completion of the spectrograph, and before any current was passed through the magnetising coils, a short zero-field run was conducted. Single muons were used for this trial, and the trigger pulse for the spectrograph was obtained from a vertical 3-fold Geiger telescope, containing 15cms of lead, placed above one arm of the magnet. The purpose of the zero-field run was to check the accuracy of the alignment of the instrument, the measurement of the flash-tube locations and the simulation technique, by examination of the symmetry and width of the scattering distribution. The width of the distribution reflects the accuracy of the simulation, and differs from the expected Coulomb scattering distribution by an amount equal to the errors due to the scattering in the trays, the measurement of the location of the flash-tubes and the simulation. A theoretical distribution for Coulomb

scattering in the magnet was obtained by calculation from a $1/p^3$ momentum spectrum of muons. This distribution is compared with the experimental results in fig.2.12. The width of the noise distribution is given by

$$\delta_{noise} = (\sigma^2_{exp} - \sigma^2_{theory})^{\frac{1}{2}}$$

which is 15', comparable with the results from the consideration of the simulation technique, from the measurements on particles that have passed through the hole in the magnet, and from the distribution of the distances below the projected half-tracks of high-energy muons at the centre level of the magnet.

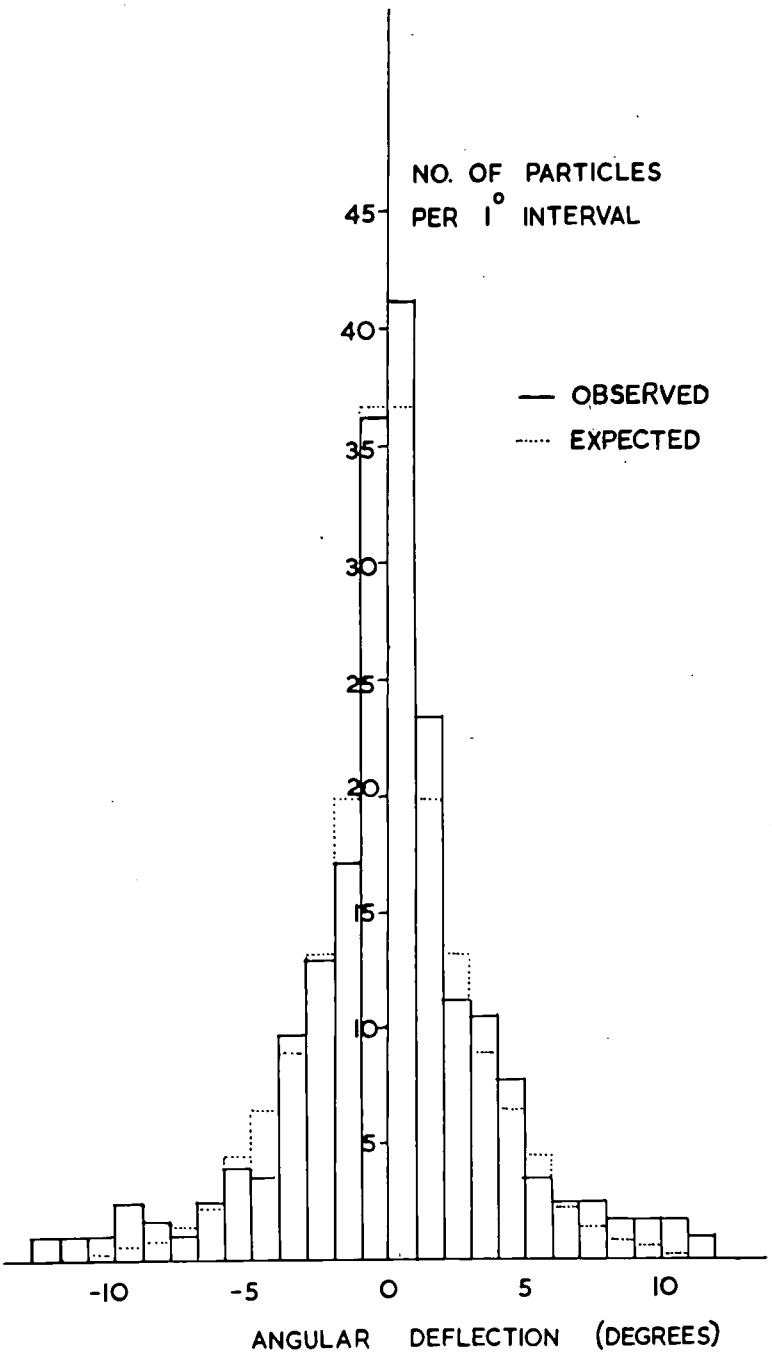
NO. OF PARTICLES
PER 1° INTERVAL
45
40
35
30
25
20
15
10
5
OBSERVED
EXPECTED
-10
-5
0
5
10
ANGULAR DEFLECTION (DEGREES)

FIG. 2.12

CHAPTER 3

THE EXTENSIVE AIR SHOWER ARRAYS

3-1 Introduction

The main Haverah Park EAS array, described by Wilson et al (1963), consists of four detecting units; one central unit with three outer units symmetrically disposed at a distance of 500m, as shown in fig 3.1. Each unit comprises 15 diffused light Cerenkov detectors of area 2·24m^2 and 120cm depth, giving a total area for each detector of 34m^2. The array records showers of about 2 x 10^7 particles at a rate of 40 per day. The mean distance of the core of the shower from the central unit is 270m, at which distance the muon density is 0·7 particles per square metre for a shower of size 2 x 10^7 particles. Thus, the number of muons incident on the sensitive area of the magnet is 50 per day, of which approximately five yield useful information of their charge and momentum.

In order to study the effects of any change in the composition of the primary cosmic radiation, suggested by Zatsepin (1963), and to investigate the characteristics of nuclear interactions at ultra-high energies, two further air-shower arrays have been constructed extending the range of detected shower sizes down to 10^5 particles. The sizes of the arrays, and the areas of the detectors, have been selected so that a complete spectrum of shower sizes from 10^5 to 10^8 particles is detected. The geometry of the new air-shower arrays is the same as the 500m array, the array spacings being 50 and

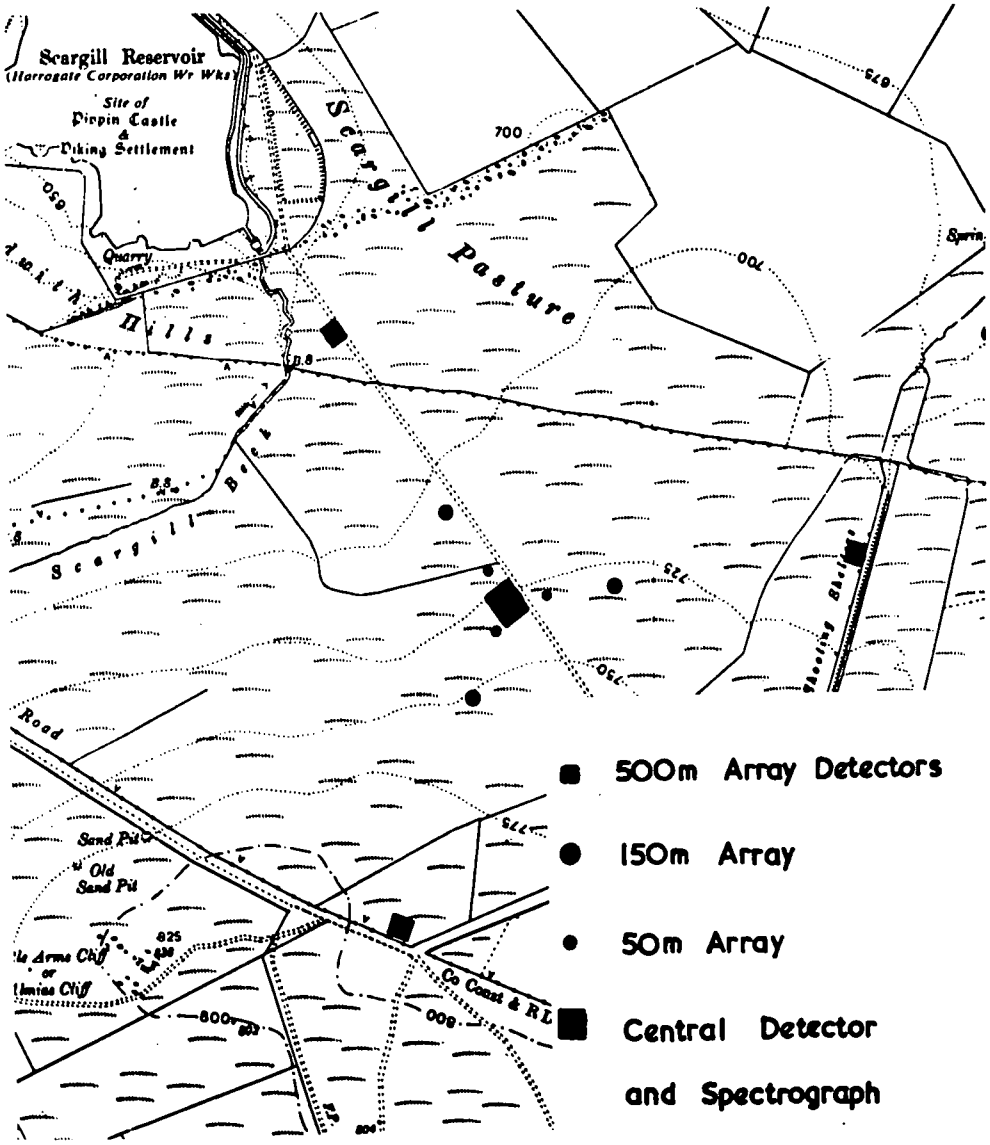
Scargill Reservoir
(Harrogate Corporation Wr Wks)
Site of
Pippin Castle
&
Viking Settlement
Quarry
Scargill Pasture
700
Scargill Beck
Road
Sand Pit
Old
Sand Pit
Co Coast & RL
500m Array Detectors
150m Array
50m Array
Central Detector
and Spectrograph

FIG. 3.1

150m. The outer detector units of the small arrays are situated along the axes of the 500m array, as shown in fig.3.1. Each unit comprises two water Cerenkov detectors of the standard design used at Haverah Park.

3-2 The Small EAS Arrays

3-2.1 The Cerenkov Detector

The Cerenkov detector, a brief description of which is given below, is described in detail by Turver (1963) and its application to air-shower detection by Lillicrap, Wills and Turver(1963). The detectors have a cubical geometry, an area of $2{\cdot}24m^2$, and a depth of 120cm ($\sim 3{\cdot}4$ radiation lengths). The water-filled tanks have a white P.V.C. ('Darvic') lining, and are operated as diffused-light Cerenkov detectors. The detector is viewed from above, using a 5" photomultiplier, EMI type 9618YB, in optical contact with the water. This configuration has the advantage of eliminating large spurious pulses arising from the Cerenkov radiation emitted when a particle traverses the photocathode, or glass envelope of the photomultiplier, and increases the light collection efficiency. The water used for the detectors has been tested for acidity and for its light transmission properties, revealing no marked difference from the sample tested by Turver (1963).

3-2.2 The Central Station

The central station comprises four of the Cerenkov detectors described above, and forms a quarter of the detector area of the 500m array central station. For economy and ease of maintenance, all power

supplies and electronic apparatus for the 50 and 150m stations, with the exception of the head-unit amplifiers of the detectors, are located at the centre of the array. Fig.3.2 is a schematic diagram of the electronic recording and calibrating apparatus, which is based on the 500m array design. The sampling system provides a continuous check of the individual tanks at a low discrimination level every $4\frac{1}{2}$ hours. An improvement incorporated in the 50 and 150m EAS arrays is the standard pulse generator, also operating at $4\frac{1}{2}$ hour intervals, which supplies a stabilised pulse to all recording channels, forming a continuous accurate check on the stability of the electronic apparatus.

3.2.3 The Recording of the Data

Two four-channel oscilloscopes are used to record the voltage pulses, and hence the particle densities, from the four detecting units in each array. To ensure accurate timing measurements, the four channels of each oscilloscope have common time-base generators and power supplies. Information on the time of arrival of the EAS front at each detector is obtained by recording the time between the rising edge of each Cerenkov detector pulse and an arbitrary mark on each channel, which is obtained by z-modulation of the time-base. Owing to the small base-line of these arrays, in particular that of the 50m array, it is only expected to distinguish between 'vertical' and 'non-vertical' showers; less than and greater than 30° from the zenith respectively. The film record of each EAS thus contains four density samples and four time of arrival measurements, together with the solar time to the

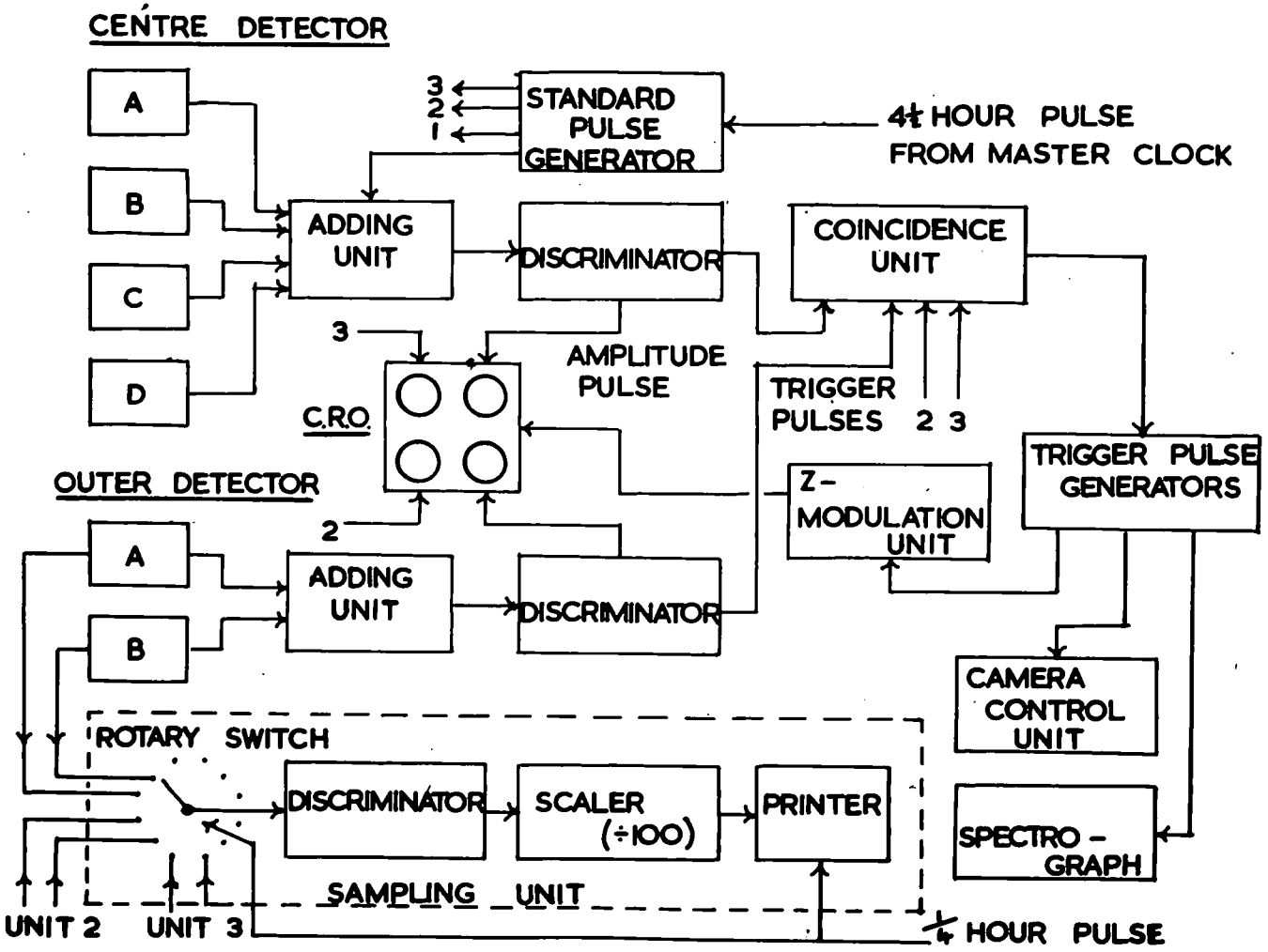
CENTRE DETECTOR
A
B
C
D
3
2
1
STANDARD PULSE GENERATOR
4½ HOUR PULSE FROM MASTER CLOCK
ADDING UNIT
DISCRIMINATOR
COINCIDENCE UNIT
3
AMPLITUDE PULSE
C.R.O.
TRIGGER PULSES 2 3
TRIGGER PULSE GENERATORS
OUTER DETECTOR
Z-MODULATION UNIT
2
A
B
ADDING UNIT
DISCRIMINATOR
CAMERA CONTROL UNIT
ROTARY SWITCH
DISCRIMINATOR
SCALER (÷100)
PRINTER
SPECTRO-GRAPH
SAMPLING UNIT
UNIT 2
UNIT 3
¼ HOUR PULSE

FIG. 3.2

nearest half-minute.

3-2.4 The Analysis of the Data

The EAS arrays each detect a small range of shower sizes, the distribution of which is very peaked. Unless they are of a systematic character, small errors in the determination of shower sizes will not result in a change in the calculated mean size for each array, which is the information required for the study of muon spectra. Consequently, a sophisticated technique of analysis is not required, and a simple programme suitable for use on the Durham Elliott 803 computer has been developed. The simplified analysis is based on the method of intersecting loci (Allan et al (1960),(1962)). As a preliminary step, a sample of the recorded air-showers incident from the vertical is analysed by analogue methods using the intersecting loci technique, assuming a lateral structure function of the form

$$D \propto r^{-n}$$

where D is the density at a distance r from the shower axis. The mean value for the exponent n is determined for these vertical showers and is found to be 2·05 for events detected by the 50m array, and 2·75 for events detected by the 150m array. Such values are consistent with the shape of the lateral structure function appropriate to the Haverah Park detector shown in fig.3.3, and based on earlier work. Because of uncertainties in the acceptance function of the spectrograph for muons incident at projected angles from the vertical greater than 30 degrees, such particles are not suitable for inclusion in the momentum spectrum. Consequently, only those showers with axes close to the vertical are required for the momentum studies, and it is possible to treat such

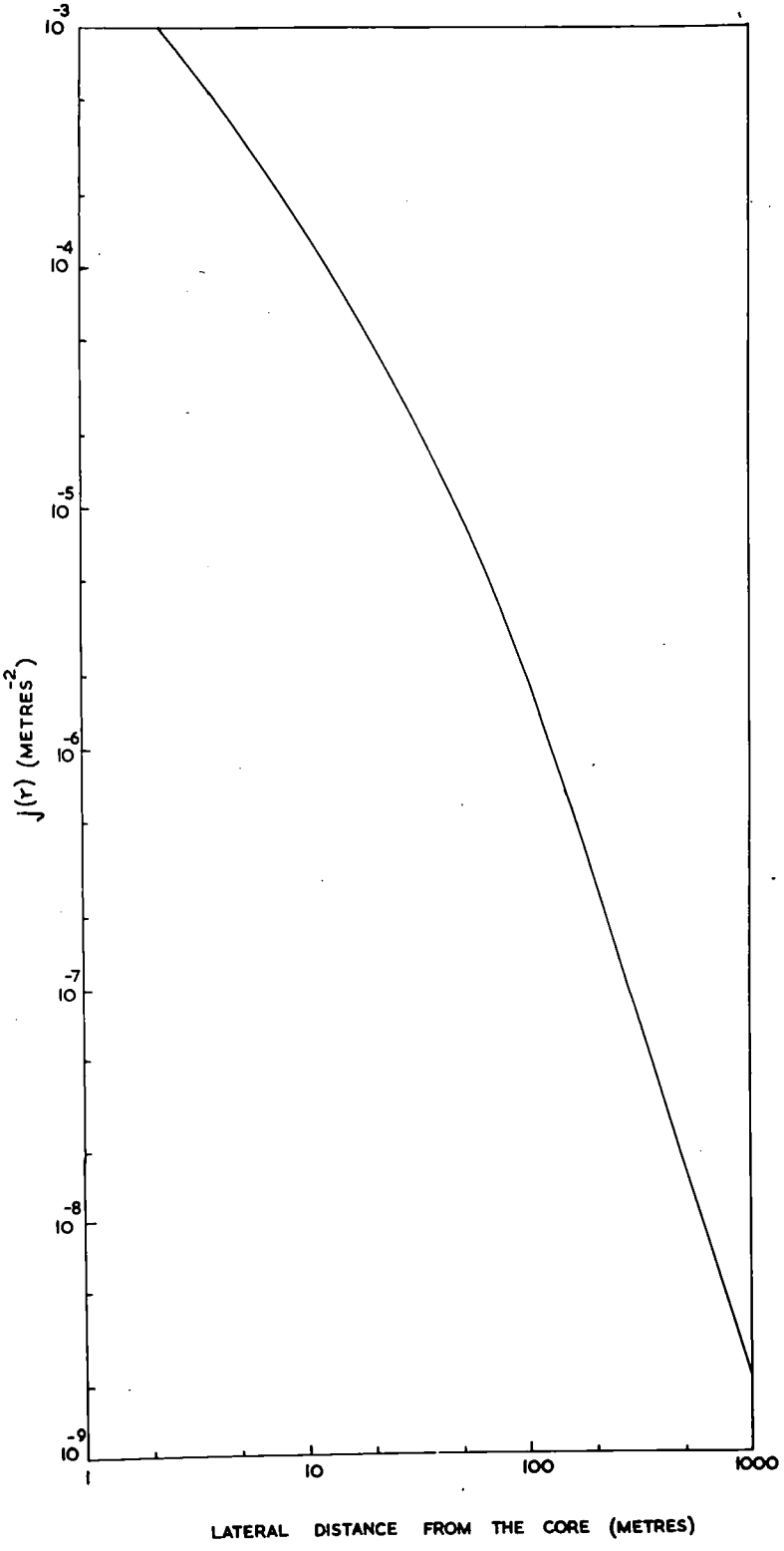
10^{-3}
10^{-4}
10^{-5}
10^{-6}
10^{-7}
10^{-8}
10^{-9}
J(r) (METRES^{-2})
1
10
100
1000
LATERAL DISTANCE FROM THE CORE (METRES)

FIG. 3.3

showers, having zenith angles up to 40°, as vertical, incurring only small errors in the determination of size and distance.

From the geometry of the arrays, it can be shown that the distance of the shower axis from the central detector is given by

$$r_1 = \frac{d\sqrt{3}}{(R_2^2 + R_3^2 + R_4^2 - 3)^{\frac{1}{2}}}$$

where $R_i = \frac{r_i}{r_1}$ r_i is the distance of the outer detector i from the from the shower axis, and d is the array spacing. From the lateral structure function,

$$\frac{r_i}{r_1} = \left(\frac{D_1}{D_i}\right)^{1/n}$$

where D_i is the recorded density at the ith detector.

Thus,

$$r_1 = \frac{d\sqrt{3}}{\left\{\left(\frac{D_1}{D_2}\right)^{2/n} + \left(\frac{D_1}{D_3}\right)^{2/n} + \left(\frac{D_1}{D_4}\right)^{2/n} - 3\right\}^{\frac{1}{2}}}$$

The shower size N is then found using the experimentally determined Cerenkov lateral structure function shown in fig.3.3, since by definition

$$D_i = N\, j(r_i)$$

The value of r found by this method is largely dependent on the highest ratio of detected densities. Consequently, a fluctuation of the shower at an outer detector will have a large effect at low densities, especially with the small detector areas involved.

A manual check of the analysed showers using the intersecting loci of the analogue method is made to ensure that all the results are meaningful. An additional safeguard is provided by comparing the observed and expected densities at three of the detectors, using a χ^2 - test.

The following information recorded by the small arrays is therefore available for the EAS which accompany muons recorded by the magnet spectrograph:-

1) Solar time (for correlation of events),
2) Total number of particles in the EAS,
3) Lateral Distance of the core from the spectrograph location (in the plane of the shower front)

3-3 The 500m Array EAS Results

The recording and analysis of the data from the 500m EAS array is carried out by workers from the University of Leeds. These results are required for detailed studies of many of the properties of EAS, and a sophisticated treatment of the data is carried out. The parameters of the EAS which are available from this analysis and which are relevant to the investigation of muons are the following:-

1) Solar time.
2) Total number of particles in the EAS.
3) Lateral distance of the core from the spectrograph location (in the plane of the shower front).
4) Co-ordinates of the point of impact of the core in the plane of the EAS array.

5) Zenith angle and azimuthal angle, defining the arrival direction of the EAS.

6) The radius of curvature of the shower front (being a measure of the height of origin of the particles).

CHAPTER 4

DERIVATION OF THE MOMENTUM SPECTRUM

4-1 Introduction

It is apparent from a consideration of the effects of the scattering of the muons in the magnet that there is no simple relation between the measured angular deflection spectrum and the incident momentum spectrum. The compensation for the noise, which gives rise to this lack of simple relation between the two spectra, can be made in two ways, both of which are used in the present analysis and provide a mutual check of their accuracy.

The first method consists of assuming an incident spectrum and applying corrections for the acceptance function of the spectrograph, the scattering and absorption in the magnet, and the magnetic deflection. The resultant deflection spectrum is then compared with the observed data by means of a χ^2 - test. This procedure is repeated, relaxing the assumed spectrum, until a satisfactory agreement is obtained.

The second method is the reverse of the above procedure, and has been derived because the shape of the incident spectrum is unknown; the first method is thus restricted to testing assumed spectra of simple shape (as described by Rochester et al (1966)). For each detected particle, the probability that it possesses a momentum p_i is evaluated from the scattering distributions for a number of values of momentum

extending across the momentum range of the spectrograph. The spectrum is then found by the summation of the probability distributions of the particles.

4-2 Evaluation of the Deflection Spectrum from an Assumed Momentum Spectrum

An outline of the procedure of this method, which has been extensively used by the Nottingham and Durham workers, will now be given. The assumed momentum spectrum, which may be represented by various functions of the power law type or by a smooth curve of a more complicated analytical form, is converted into a histogram with cells having a median value p_i and containing approximately equal numbers of particles.

The acceptance characteristics of the spectrograph $M_1(p_i, \gamma_o, \phi_o)$, expressed as a function of the incident direction of the particle, specified by the angle in the measuring plane, γ_o, and the angle ϕ_o in the vertical plane perpendicular to the measuring plane, and the momentum p_i, is derived using the analytical method described in section 2.6.3. This is used to correct the observed distributions of initial directions $M_2(\gamma_o)$, $M_3(\phi_o)$, where ϕ_o is found from the associated air-shower data, and is accurate to $\pm 5^\circ$ in the case of the 500m array. Hence,

$$A_i(\gamma_o, \phi_o) = M_1(i, \gamma_o, \phi_o) \cdot M_2(\gamma_o) \cdot M_3(\phi_o),$$

where $A_i(\gamma_o, \phi_o)$ is the corrected distribution, expressed as a function of the momentum p_i. The magnetic deflection $\Delta\gamma_m$ is

computed for each value of p_i, $(\psi_o)_k$, and $(\phi_o)_l$, where $(\psi_o)_k$ and $(\phi_o)_l$ are the medium values of the cells in the corresponding histograms of observed incident angles, using the relation

$$l = \frac{p_i}{\epsilon} \sin\psi_o \sin\omega \left(e^{-(\psi-\psi_o)\tan\omega} \sin(\psi-\omega) - \sin(\psi_o-\omega)\right),$$

where ϵ is the specific energy loss in MeV/cm, as quoted by Ashton et al (1963). l is the magnet thickness, expressed in cm, and

$$\omega = -\tan\frac{\epsilon c}{e H_o}$$

The expected number of muons in the jth interval of the observed deflection spectrum is then derived using the expression

$$\langle N_j \rangle = \sum_i s(p)\, dp\, g_{ji},$$

where $s(p)\,dp$ is the assumed differential spectrum and the 'weighting factor' g_{ji} is given by

$$g_{ji} = \sum_k \sum_l A_i(k,l)\; G(i, k, l, j),$$

and $G(i, k, l, j)$ is the probability that a particle of momentum p_i, incident at angle $(\psi_o)_k$ and $(\phi)_l$ will be deflected by $(\Delta\psi)_j$, taking into account the scattering in the magnet and the errors of track location. G is thus a Gaussian function of standard deviation σ_G, where $\sigma_G^2 = \sigma_s^2 + \sigma_{exp}^2$,

and $$(\sigma_s)^2_{i,k,l,j} = \frac{21 \times 10^{-3} \times (S^{\frac{1}{2}})_{kl}}{\sqrt{2}\,\beta\, c\,(p_i - \epsilon S)},$$

in which S is the path length in the magnet.

This procedure is repeated for all values of p_i. The

distributions are then weighted in proportion to the intensities of $S(p_i)$ making up the assumed spectrum, thus giving the deflection spectrum, which is to be compared with the observed data.

4-3 The Derivation of the Incident Momentum Spectrum from the Observed Deflections

For each recorded particle, information is available on its incident direction, ψ_o and ϕ_o, and selected values of momentum extending across the sensitive range of the spectrograph; the associated magnetic deflection $\Delta\psi_m$ is calculated using an iterative computer programme to solve the relation given by Eyges (1948):-

$$p_i = \frac{1k\ (\ 1 + \epsilon^2/k^2\ )}{\exp\left\{\frac{\epsilon}{k}\ \Delta\psi_m\right\}(\sin\psi_m + \frac{\epsilon}{k}\cos\psi_m) - (\sin\psi_o + \frac{\epsilon}{k}\cos\psi_o)}\ ,$$

where k = 300 x the magnetic induction, ϵ is the specific energy loss, l the magnet thickness, and $\psi_m = \psi_o + \Delta\psi_m$.

The probability $G(p_i, \Delta_i)$ of the particle having a momentum p_i and being scattered through an angle Δ_i given by

$$\Delta_i = (\Delta\psi - \Delta\psi_m)$$

is found using the expression for the standard deviation of the scattering distribution about ψ_m :-

$$\sigma_G = \left\{\frac{E_s^2 \times S}{2\ p_i\ (p_i - \epsilon S)} + \sigma_{exp}^2\right\}^{\frac{1}{2}}\ ,$$

where $E_s = 21 \times 10^6$ eV, and S is the path length of the particle of

momentum p_i, incident angle ψ_o, undergoing only magnetic deflection.

The probability distribution $G(p_i, \Delta_i)$ is correct only for a spectrum having equal numbers of particles of all momenta, and so a correction to $G(p_i, \Delta_i)$ is made to account for the shape of the spectrum. The probability of a particle $(\psi_o, \phi_o, \Delta\psi)$ having a momentum p_i is thus:-

$$P = \frac{G(p_i, \Delta_i)\ S(p_i)\ dp_i}{\int_{p_{min}}^{p_{max}} G(p_i, \Delta_i)\ S(p_i)\ dp_i} ,$$

where $S(p_i)$ is the expected intensity of the momentum spectrum at p_i, p_{min} is the lowest momentum accepted by the magnet, p_{max} is unknown, but is taken to be a value larger by a factor of two than the upper limits of the results quoted. The normalised distribution is then divided by the probability of acceptance by the spectrograph of that particle, $Y(\psi_o, \Delta\psi)$. Thus, the total probability is given by

$$P' = \frac{G(p, \Delta)\ S(p)\ dp}{Y(\psi_o, \Delta\psi) \int_{p_{min}}^{p_{max}} G(p, \Delta)\ S(p)\ dp}$$

The distributions for a number of particles are then summed to give the differential spectrum appropriate to the sample of particles. Although the procedure is expected to be iterative, it is found to be

very insensitive to the form of the 'trial spectrum', S(p) dp, used to correct the probability function $G(p, \Delta)$. In order to simplify the correction for the low momentum particles incident at large angles, for which the acceptance function is very imprecise, a cut-off is applied to ψ_0 and $\Delta\psi$. The limits imposed ($\Delta\psi = 16^\circ$, $\psi_0 = 30^\circ$) are equivalent to a mean momentum of 1·7 GeV/c. Each value of the spectrum at low momenta is corrected for the probability of being scattered beyond the cut-off value of $\Delta\psi$. The probability of exclusion is one-half at a momentum of 1·7 GeV/c, decreasing to a negligible value at 2 GeV/c. The cut-off values also specify the maximum track length and hence the minimum detectable momentum (1·5 GeV/c) at which absorption has no effect, and so no correction for absorption in the magnet is necessary above this value. In practice, no correction for absorption in the magnet is made in this treatment, and the shape of the spectrum below 1·7 GeV/c is found using the first, inverse, method of analysis, with the fixed shape of the spectrum determined by this procedure above the cut-off value, and the best shape below the cut-off value found by a systematic relaxation method.

4-4 Comparison of the Two Methods for the Derivation of the Momentum Spectrum

The two methods of analysis of the data use acceptance functions for the spectrograph and expressions for the deflections due to the magnetic field and scattering in the magnet material which are derived from entirely independent sources. As a test of the

procedures, the data representing the whole of the information from the 500m array has been processed by the second method, and the resulting momentum spectrum converted back to a deflection spectrum by the first method. The comparison between the experimentally observed deflection spectrum and the "theoretical" spectrum is made in fig.4.1.

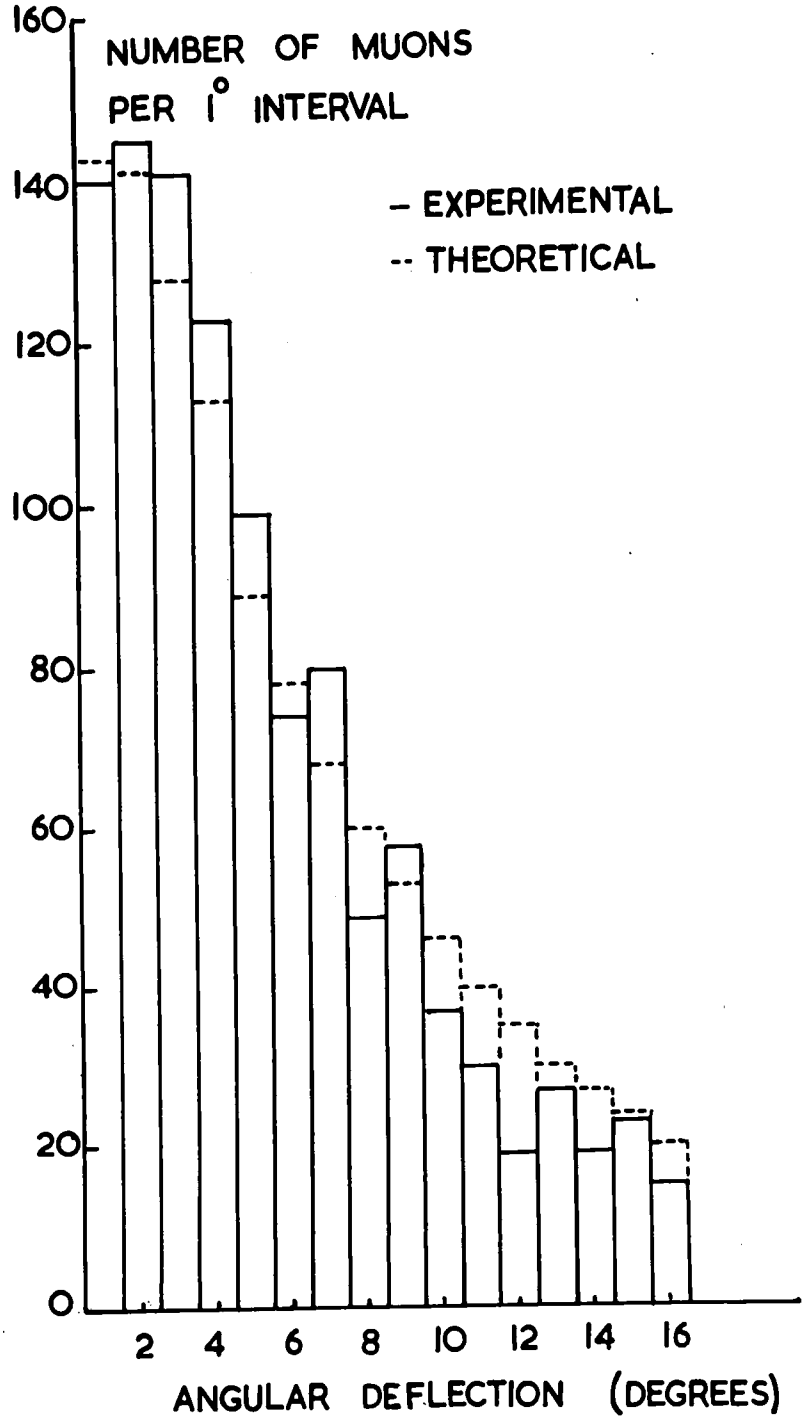
160
140
120
100
80
60
40
20
0
NUMBER OF MUONS
PER 1° INTERVAL
– EXPERIMENTAL
-- THEORETICAL
2
4
6
8
10
12
14
16
ANGULAR DEFLECTION (DEGREES)

FIG. 4.1

CHAPTER 5

THE MOMENTUM SPECTRUM OF MUONS IN EAS

5-1 Interpretation of Data and Results

5-1.1 The Absolute Differential Momentum Spectrum in EAS of Size 2×10^7 Particles

The measured angular deflections of the recorded muons have been classified according to the distances of the associated EAS cores from the spectrograph. Seven intervals of distance in the range 37 to 610m have been used and the shape of the differential spectra derived using the methods described in sections 4.2 and 4.3. Typical distributions of the size, lateral distance from the core, and zenith angles for the showers accompanying the muons contributing to a spectrum are shown in figs. 5.4, 5.5 and 5.6 respectively for the spectrum at 300m.

An experimental determination of the lateral distribution function $f_\mu(r)$ for the muons of momentum $p \geq 1$ GeV/c in the EAS arriving with zenith angles less than 40° has been made using tray B3 as a detector and the magnet iron as absorber. The spectra obtained by the procedures described in sections 4.2 and 4.3 have been integrated analytically up to a momentum of 1,000 GeV/c (a 10% increase is incurred if the integration is continued to infinite momentum), and the factor required to convert the spectrum to absolute densities has been found for each lateral distance from the core by comparison with the lateral distribution function.

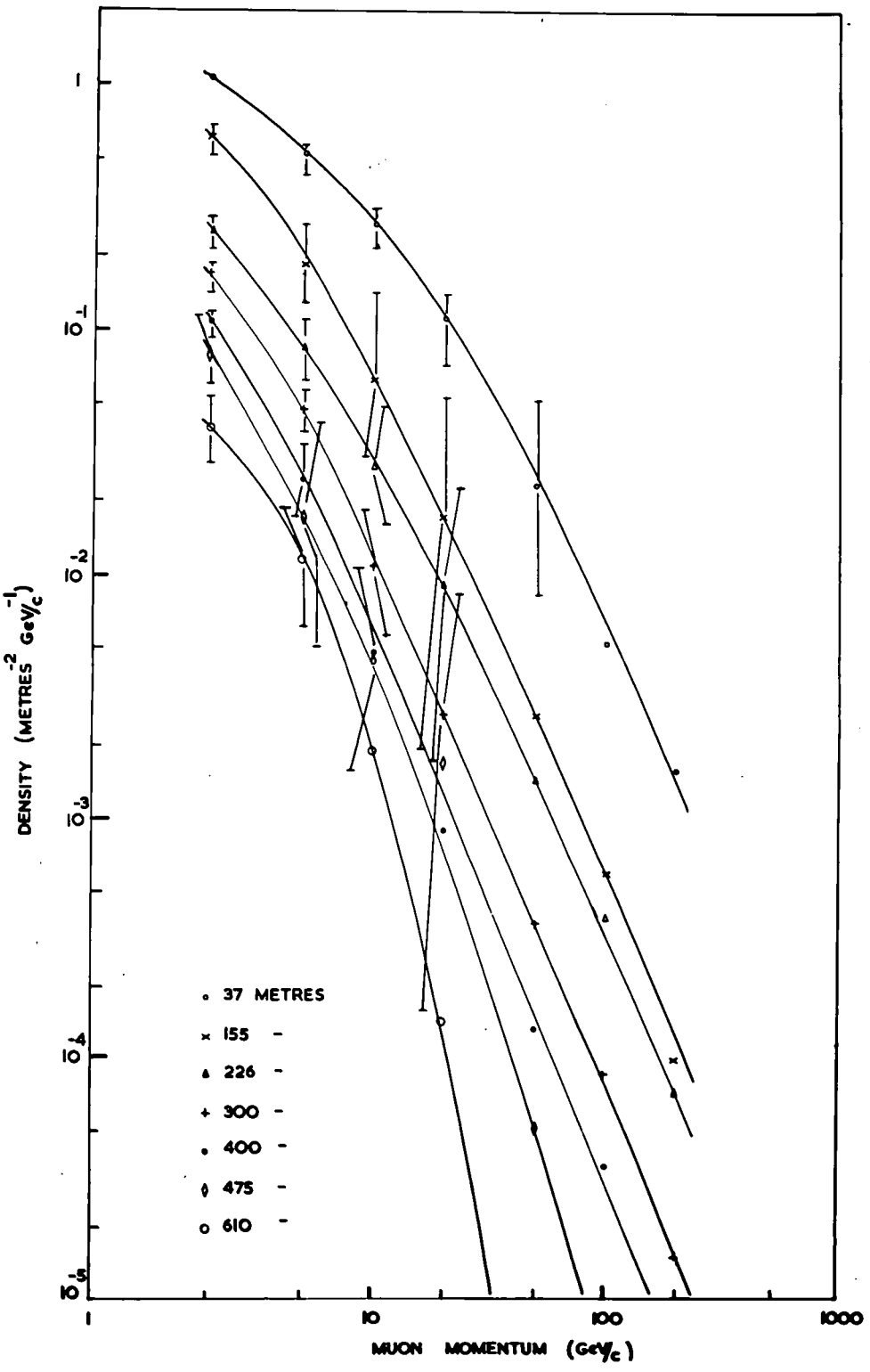
DENSITY (METRES^{-2} GeV/c^{-1})
1
10^{-1}
10^{-2}
10^{-3}
10^{-4}
10^{-5}
1
10
100
1000
MUON MOMENTUM (GeV/c)
37 METRES
155 -
226 -
300 -
400 -
475 -
610 -

FIG. 5.1

In the case of the 37m spectrum, which is based on data recorded in showers of size 4×10^5 particles, a normalisation from $N = 4 \times 10^5$ to 2×10^7 particles has been made using the results of an experimental determination of the dependence of the muon densities for $p \geqslant 1$GeV/c on shower size N from the absorption experiment. The dependence is found to be

$$N_\mu \propto N^{0.77 \pm 0.08} \quad \text{(Earnshaw (1966))},$$

and recent results from this experiment indicate the validity of this relation for all momenta. The absolute differential momentum spectrum $s(p)\,dp$ is shown in fig. 5.1.

5-1.2 The Mean Momentum of the Muons in an EAS as a Function of the Lateral Distance from the Core.

The total momentum flux density, given by

$$q(r) = \int_0^{1000} S(p).p\,dp,$$

in an EAS at a distance r from the core has been evaluated for each interval of r, and the mean momentum $\bar{q}(r)$ found from the integral density of muons at r ; the results are shown in fig. 5.8.

5-1.3 The Absolute Integral Momentum Spectrum of Muons in EAS of Size 2×10^7 Particles

The shape of the integral momentum spectrum at a distance r from the EAS has been normalised to the integral density $\geqslant 1$ GeV at r, measured in the absorption experiment, with the necessary scaling of the measurements made at a shower size of 4×10^5 particles up to a size of 2×10^7 particles. The absolute integral momentum spectra

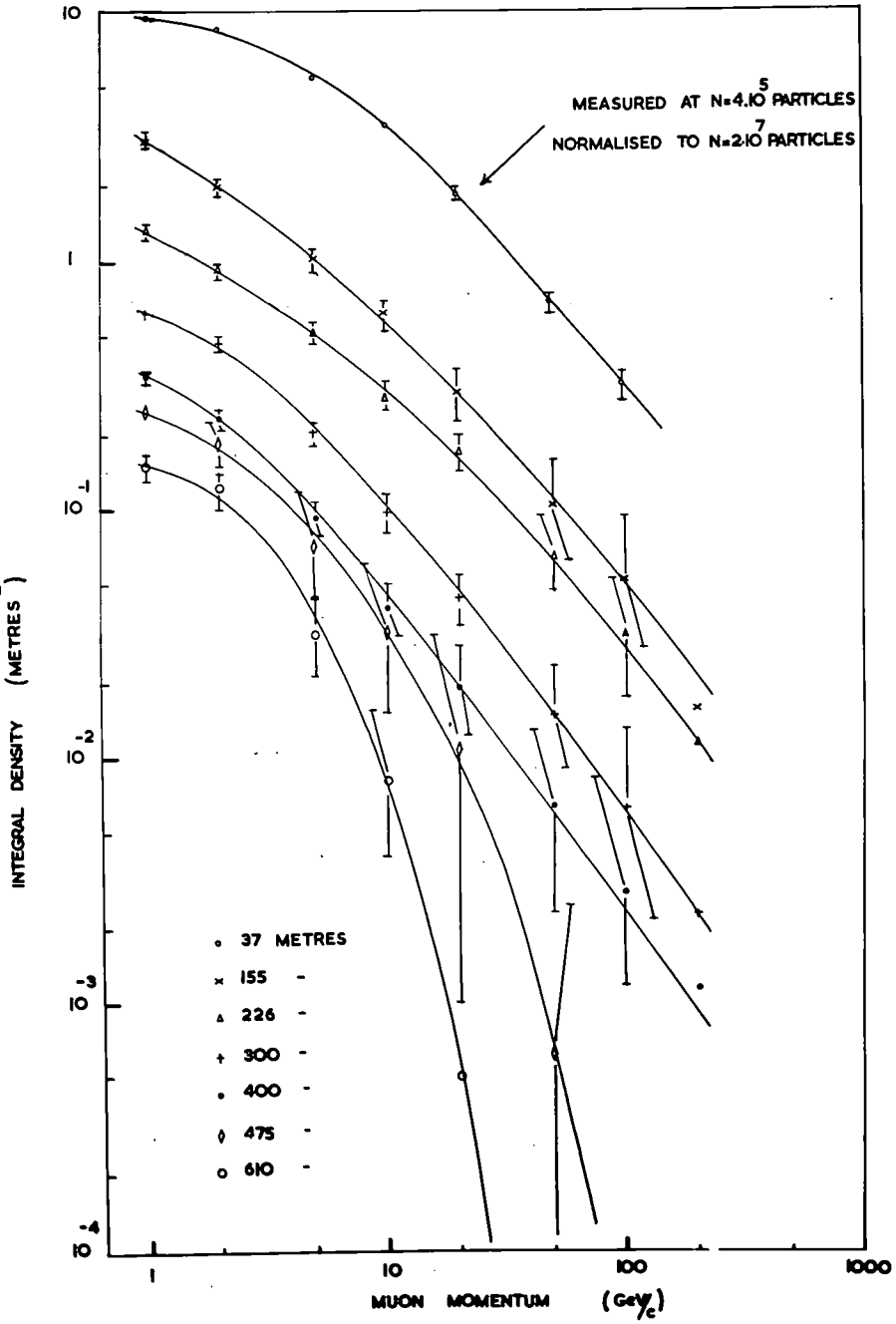
MEASURED AT N=4.10^5 PARTICLES
NORMALISED TO N=2.10^7 PARTICLES
37 METRES
155 -
226 -
300 -
400 -
475 -
610 -
INTEGRAL DENSITY (METRES^-2)
MUON MOMENTUM (GeV/c)
10
1
10^-1
10^-2
10^-3
10^-4
1
10
100
1000

FIG. 5.2

for a shower of size 2 x 10^7 particles are shown in fig. 5.2.

5-1.4 The Lateral Distribution Function of Muons

It is often more convenient to represent the experimental data in the form of the lateral distributions of muons in EAS with momentum $\geqslant p$, $f_\mu(r, \geqslant p)$. From the integral spectra, the lateral distributions of mu-mesons as a function of the momentum have been derived and are shown in fig. 5.3. The errors on the observations, which are identical with those of the integral spectra, have been omitted for clarity.

5-1.5 The Total Momentum carried by Muons in EAS of Size 2 x 10^7 Particles

The total momentum carried by the muon component in the shower is given by

$$Q_T = \int \bar{q}\,(r)\, f_\mu(r)\, 2\pi r\, dr,$$

where the integral is evaluated from 1m to 1,000m, since the contribution of muons outside these limits is negligibly small. The form of $f_\mu(r)$ for distances less than 10m, which is assumed in the integration, is indicated by the broken lines in fig.5.3. The total momentum carried by the muon component in an EAS of size 2 x 10^7 particles evaluated from the integral is found to be 1·08 x 10^7 GeV/c

The total number of muons in a shower of size 2 x 10^7 particles is found by evaluating the integral

$$N_\mu(r, \geqslant p) = \int f_\mu(r, \geqslant p)\, 2\pi r\, dr,$$

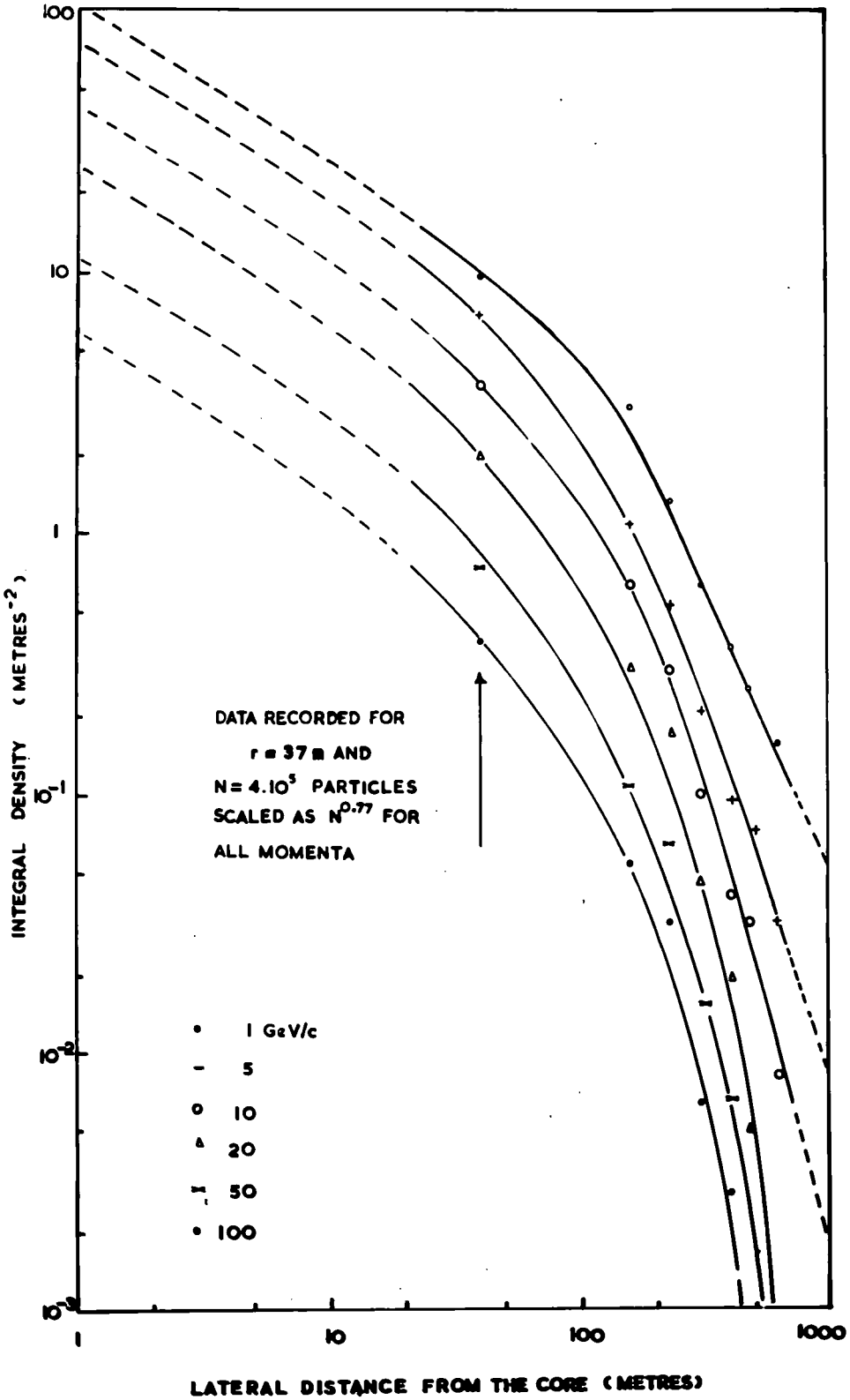
100
10
1
10^{-1}
10^{-2}
10^{-3}
INTEGRAL DENSITY (METRES^{-2})
DATA RECORDED FOR
r = 37 m AND
N = 4.10^5 PARTICLES
SCALED AS N$^{0.77}$ FOR
ALL MOMENTA
1 GeV/c
5
10
20
50
100
1
10
100
1000
LATERAL DISTANCE FROM THE CORE (METRES)

FIG. 5.3

for several values of p, and plotting N_μ as a function of $(p + 2)$ GeV/c. The momentum distribution of muons in an EAS of size 2×10^7 particles is shown in fig. 5.7, and the total number of muons with momentum greater than zero has been found by an extrapolation of the curve to the point where $(p + 2) = 2$. This gives the integral number of muons as $1{\cdot}8 \times 10^6$ particles, yielding a value of 6·0 GeV/c for the average momentum of all muons in the shower.

5-2 Comparison with Earlier Measurements

The integral spectra for muons in EAS found by Andronikashvili et al (1960), Vernov et al (1960), and Dovzhenko et al (1957) are shown in fig. 1.1. The results of the present experiment are in good agreement with the two exponent curve given by Andronikashvili et al for a lateral distance from the core of 28m in a shower of size $2{\cdot}9 \times 10^5$ particles, and the spectrum at 300m found by Dovzhenko et al. The spectra at 100m given by Dovzhenko et al and Vernov et al are both much harder than the spectrum at 155m shown in fig. 5.2.

Fig. 1.2 shows the integral spectra found in the absorption experiment of de Beer et al (1962), which are much steeper than the present results, and are nearly indistinguishable for lateral distances from the core of 100 to 300m.

The shapes of the integral spectra of Bennett and Greisen (1961) shown in fig.1.2, are in very good agreement with the results of the present experiment, over the momentum range in which comparison between the two experiments is possible. Bennett and Greisen have given an

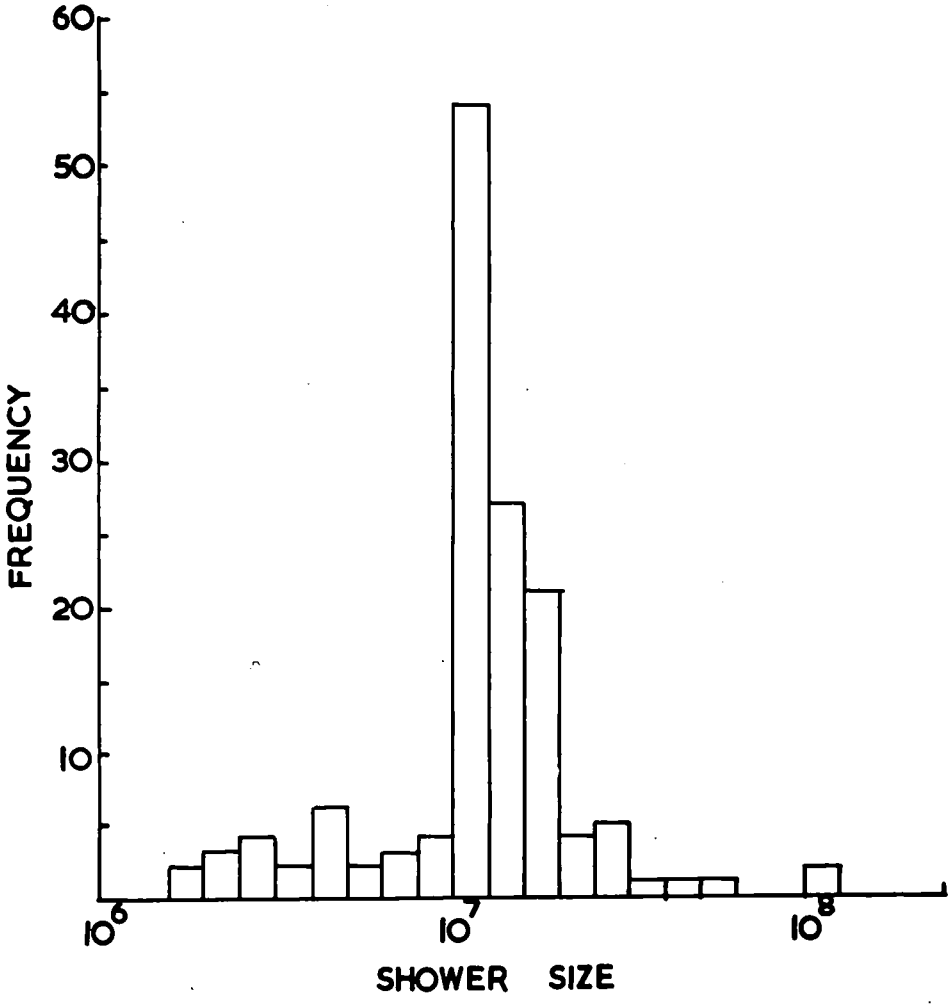

FIG. 5.4

empirical function relating the integral density of muons with the shower size and lateral distance from the core, which is a good fit to their data and incorporates the measurements of Clark et al (1958) for $p \geqslant 1{\cdot}2$ GeV/c :-

$$\rho_\mu(N,r,\geqslant p) = \frac{14{\cdot}4\, r^{-0{\cdot}75}}{(1 + \frac{r}{320})^{2{\cdot}5}} \left(\frac{N}{10^6}\right)^{0{\cdot}75} \left(\frac{51}{p+50}\right) \left(\frac{3}{p+2}\right)^{0{\cdot}14r^{0{\cdot}37}}$$

where ρ_μ is the average number of muons per square metre with momentum exceeding p GeV/c at r metres from the core of a shower of size N particles. Evaluation of this expression for a shower of size 2×10^7 particles yields densities which are lower than those found in the present experiment. A corresponding discrepancy is found in the value of $1{\cdot}23 \times 10^6$ muons in a shower of size 2×10^7 particles, found by Bennett and Greisen, compared with the present value of $1{\cdot}8 \times 10^6$ muons. Since the present data is not in disagreement with the integral densities for $p \geqslant 1{\cdot}2$ GeV/c as given by Clark et al (1958), it is difficult to trace the source of the discrepancy.

5-3 Comparison with Theoretical Models

The momentum spectra have been compared with the recent theoretical models of Holyoak et al (1966) and Hillas (1966).

The assumptions made by Holyoak et al are that the proton interaction length is 80 gm cm^{-2}, the inelasticity of the proton - nucleon and pion-nucleon interaction are equal to 0·5 and independent of energy. The probability of the decay of nucleons and the energy

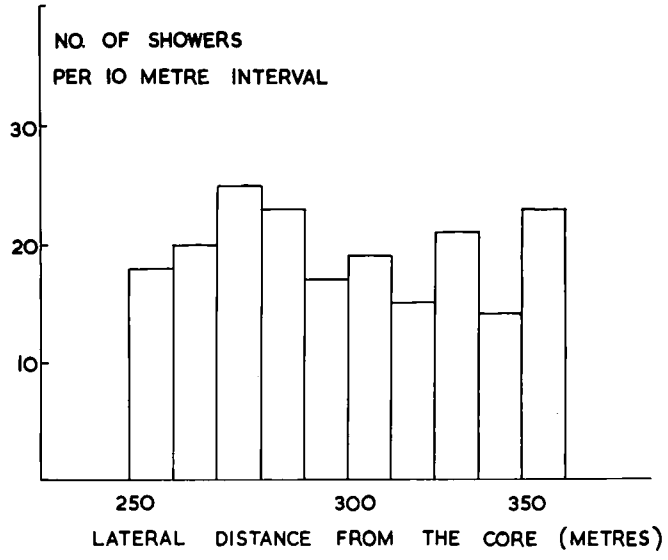
NO. OF SHOWERS
PER 10 METRE INTERVAL
30
20
10
250
300
350
LATERAL DISTANCE FROM THE CORE (METRES)

FIG. 5.5

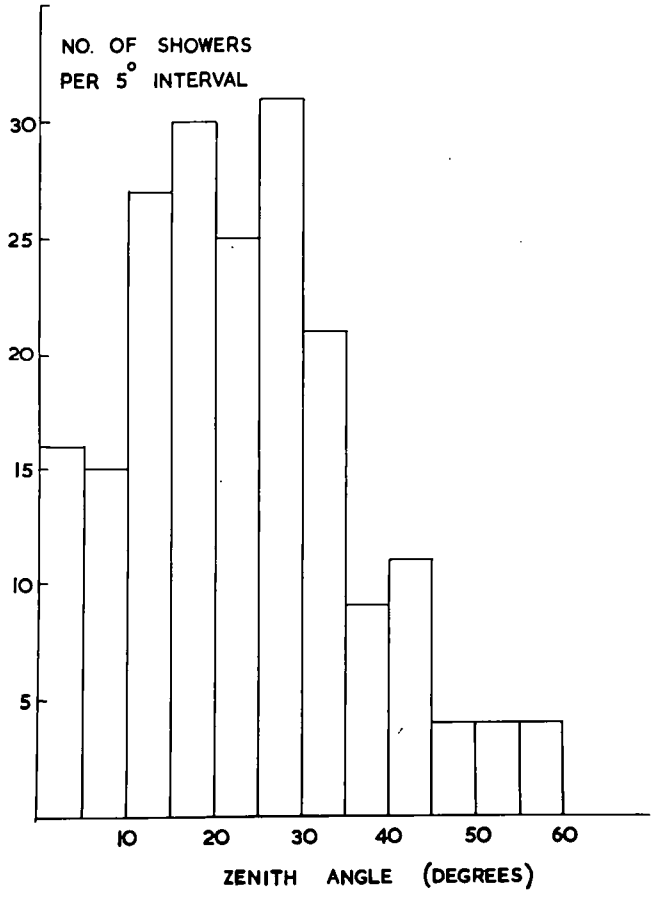
NO. OF SHOWERS
PER 5° INTERVAL
30
25
20
15
10
5
10
20
30
40
50
60
ZENITH ANGLE (DEGREES)

FIG. 5.6

loss of the muonic component is taken into account, and the energy of a muon produced by the decay of a pion was assumed to be 0·76 times the energy of the muon. The energy spectrum and angular distribution of the secondaries from the proton-nucleus collision are of the same form as the CKP model, and are similar to the distributions used by Hillas. The model by Hillas also assumes that the muons are produced on the shower axis, and a correction is made for the lateral displacement of muons by the Earth's magnetic field, making possible the deduction of the heights of origin of muons of various energies.

The integral spectra predicted by both models are much steeper than found in this experiment: the number of muons at 100m with momentum greater than 10 GeV/c is found to be 12 particles per square metre in the present experiment, while the model of Holyoak et al predicts 5×10^{-2} particles per square metre. The predicted variation of mean momentum with the lateral distance from the core of the shower given by Holyoak et al is plotted on fig. 5.8 for comparison with the results of the present experiment; reasonable agreement can be found between theory and experiment at distances beyond 100m from the core, although the theory generally yields higher values than those found experimentally.

The discrepancy between the steep lateral distributions predicted by the models and the experimental data may be explained by a high momentum tail to the transverse momentum distribution of the pions. An alternative explanation is that the muon cascade maximum

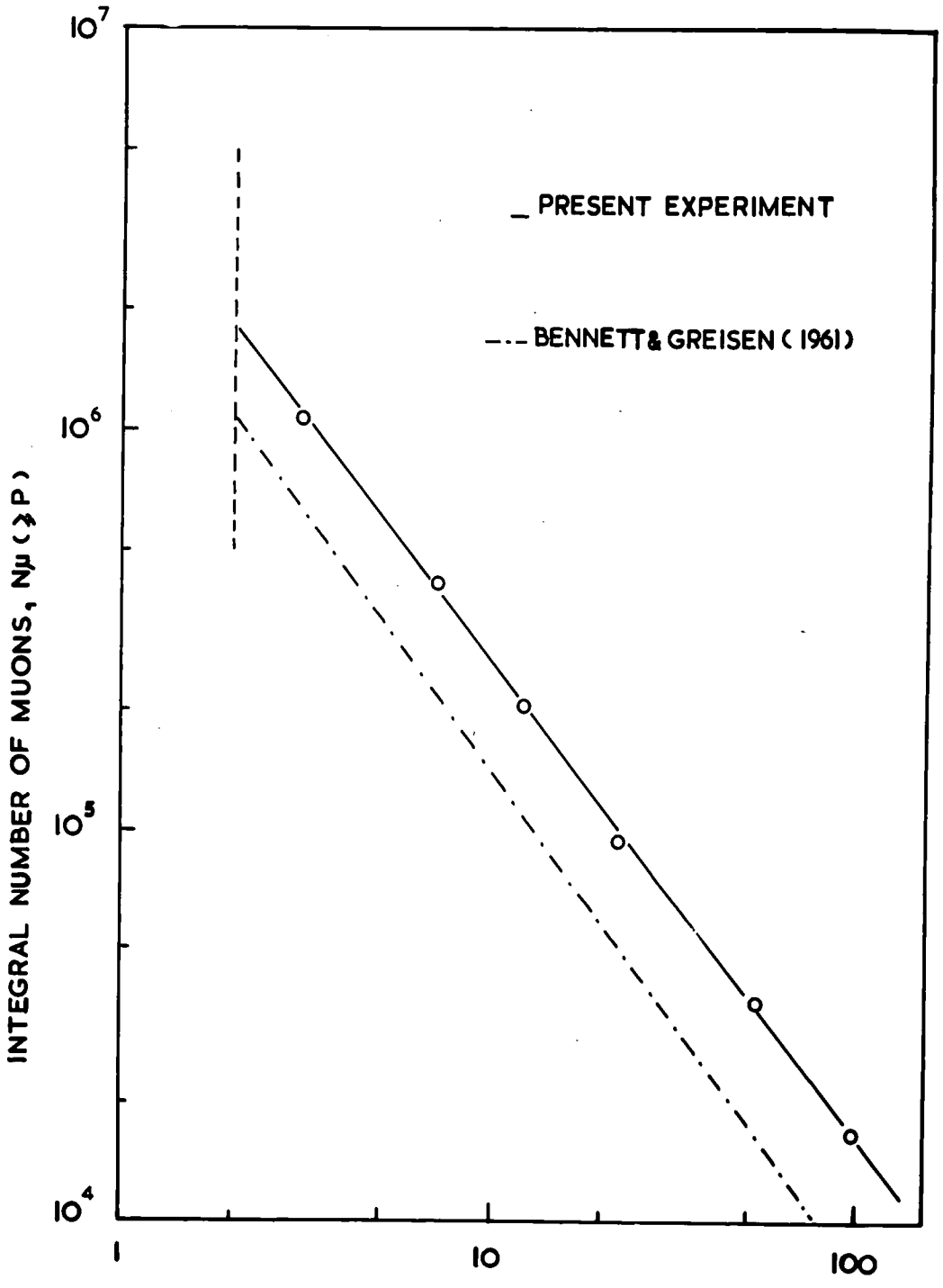
10^7
10^6
10^5
10^4
PRESENT EXPERIMENT
BENNETT & GREISEN (1961)
INTEGRAL NUMBER OF MUONS, $N_\mu (\geq P)$
1
10
100
MUON MOMENTUM , P+2 (GeV/c)

FIG. 5.7

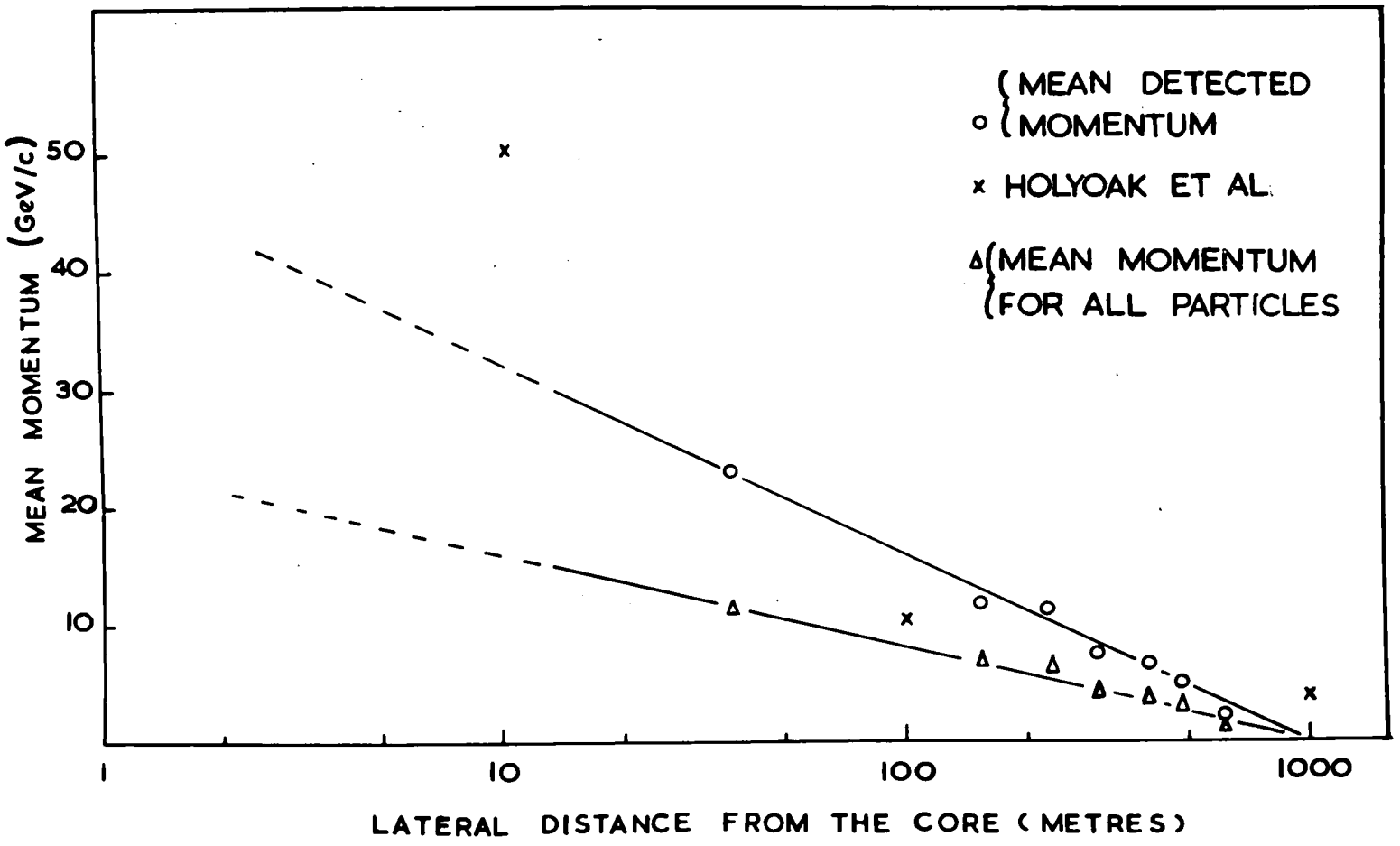
MEAN DETECTED MOMENTUM
HOLYOAK ET AL.
MEAN MOMENTUM FOR ALL PARTICLES
MEAN MOMENTUM (GeV/c)
50
40
30
20
10
1
10
100
1000
LATERAL DISTANCE FROM THE CORE (METRES)

FIG. 5.8

occurs higher in the atmosphere than is assumed in the models, a general conclusion in line with much of the data presented at the 1965 IUPAP Conference. The presence of high energy kaons, which are not considered in either theoretical approach, and which have a higher transverse momentum and total energy, and a longer lifetime than the pions, may also account for the larger number of high energy muons.

It may be noted that the number of muons of momentum $p \geqslant 1$ GeV/c in a shower of size 2×10^7 particles ($1{\cdot}07 \times 10^6$) is considerably higher than the predicted total of 4×10^5 mu-mesons for a primary energy of 5×10^7 GeV, given by Holyoak et al , which is also lower than the value of $6{\cdot}6 \times 10^5$ found by Bennett and Greisen (1961).

5-4 Further Work on the Muon Component in EAS

The possible explanations of the discrepancies between the theoretical models and the experimental results, which are outlined in section 5-2, indicate the characteristics of muons in EAS which still need to be measured accurately. The establishment of a more statistically significant lateral distribution function for muons of momentum $\geqslant p$ from the extended operation of the present experiment will result in a firmer indication of the transverse momentum of the parent pions. A logical continuation of this work is the extension of momentum measurements on muons in EAS to higher energies, using underground muon detectors in conjunction with a large air shower array on the surface. (see eg. Chatterjee et al (1966)). An indication of the contribution of kaons to the muon component, which is neglected in the theoretical models,

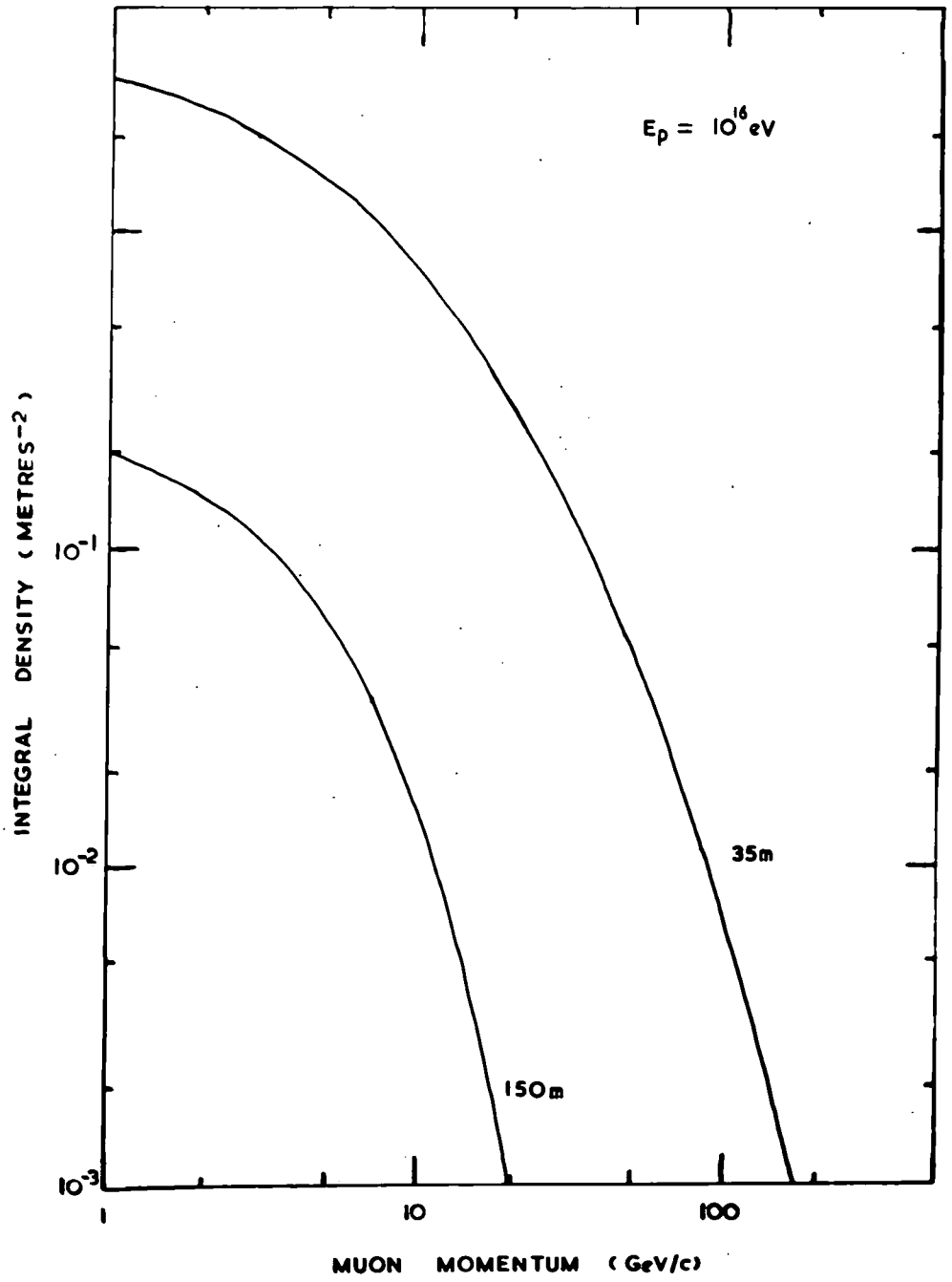
$E_p = 10^{16}$ eV
35m
150m
INTEGRAL DENSITY (METRES^{-2})
10^{-1}
10^{-2}
10^{-3}
1
10
100
MUON MOMENTUM (GeV/c)

FIG. 5.9

Coates,D.W., 1961, Ph.D. Thesis, University of Nottingham.

Cocconi,G., 1958, Phys.Rev., 111, 1699.

Cocconi,G., Koester,L.J., and Perkins,D.H., 1961, High Energy Study Seminars, University of California.

Conversi,M., and Gozzini,A., 1955, Nuovo Cim., 2, 189.

Coxell,H., and Wolfendale,A.W., 1960,Proc.Phys.Soc., 75, 378.

De Beer,J.F., Cranshaw,T.E., and Parham,A.G., 1962,Phil.Mag., 7, 499.

Dedenko,L.G.,1966, Proc.London Conf.Cosmic Rays. To be published.

Dovzhenko,O.I., Nelepo,B.A., and Nikolskii,S.I., 1957, Sov.Phys. J.E.T.P., 5, 391.

Earnshaw,J.C., 1966, To be published.

Euler,H., and Wergeland,H., 1940,Astrophys. Norveg, 3, 1965. Naturwissenschaften, 23, 41.

Eyges,L., 1949, Phys.Rev., 74, 1534.

Fermi,E., 1950, Progr.Theor.Phys., 5, 570.

Fukuda,M., Ueda,N., and Ogita,A., 1959, Prog.Theor.Phys., 21, 29.

Gardener,M., Kisdnasamy,S., Rössle,E., and Wolfendale,A.W.,1957, Proc.Phys.Soc., B, 70, 687.

Greisen,K., 1956, Progress in Cosmic Ray Physics,III, 1. 1960, Ann.Rev.Nucl.Sci., 10, 63.

Hayman,P.J., and Wolfendale,A.W., 1962, Proc.Phys.Soc., 80, 710.

Heisenberg,W., 1952, Z.Phys., 133, 65.

Hillas,A.M., 1966, Proc.London Conf. Cosmic Rays. To be published.

Holmes,J.E.R., Owen,B.G., and Wilson,J.G., 1961, Proc.Phys.Soc., 78, 496.

Holyoak,B., Thompson,M.G., and Wdowczyk,J., 1966, Proc.London Conf. Cosmic Rays. To be published.

Hyams, B.D., Mylroi,M.G., Owen,B.G., and Wilson,J.G., 1950, Proc.Phys. Soc., A63, 1053.

Janossy,L., and Messel,H., 1951, Proc.Roy. Irish Acad., A, 54, 217.

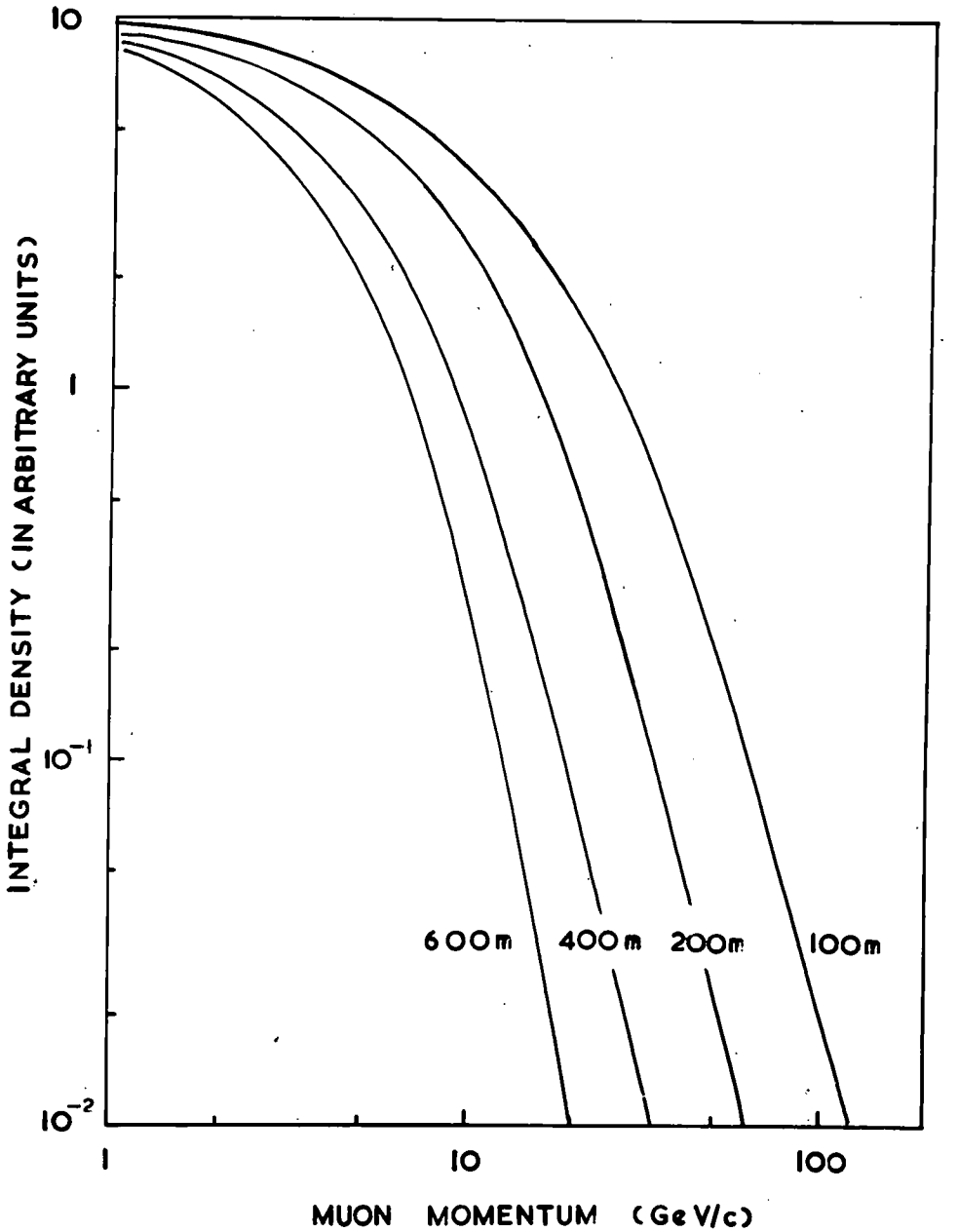
10
1
10^{-1}
10^{-2}
INTEGRAL DENSITY (IN ARBITRARY UNITS)
600m
400m
200m
100m
1
10
100
MUON MOMENTUM (GeV/c)

FIG. 5.10

will be provided by the positive to negative ratio of the detected muons in the air-showers, The presence of kaons in large numbers may account for the observed number of high energy muons at large lateral distances from the air-shower core. The extension of the present measurements of the momentum spectra to smaller shower sizes ($\sim 10^4$ particles) would be relevant, since it would allow a more direct comparison with models based directly on the results of accelerator and emulsion experiments.

The height of production of the muons may possibly be found using the technique of shower front analysis employed by Baxter et al (1966), the width of the shower front indicating whether the detected particles originate in a single efficient collision process, or in several relatively inefficient collisions over a large region of the atmosphere. It may also be possible to measure the mean height of production of the muons from the measurement of their angular dispersion using accurate track locators, such as neon flash tube arrays, possibly with momentum determination, separated by a large distance. A third method for the estimation of the height of production of muons is provided by the displacement of the positive and negative mu-mesons by the Earth's magnetic field. The height of production of the parent pions is given by the magnitude of the east-west asymmetry in the EAS.

REFERENCES

Alkofer,O.C., 1960, Z.Phys., 158, 274.

Allan,H.R., Beamish,R.F.W., Bryant,D.A., Kasha,H., and Wills,R.D., 1960, Proc.Phys.Soc., A, 76, 1.

Allan,H.R., Beamish,R.F.W., Glencross,W.M., Thomson,D.M., and Wills,R.D., 1962, Proc.Phys.Soc., A, 79, 1170.

Andronikashvili,E.L., and Kazarov,R.E., 1960, Proc.Moscow Conf. Cosmic Rays, II, 149.

Ashton,F., Nash,W.F., and Wolfendale,A.W., 1959, Proc.Roy.Soc., A, 253, 163.

Ashton,F., Mackeown,P.K., Pattison,J.B.M., and Wolfendale,A.W., 1963, Proc.Jaipur Conf. Cosmic Rays, 6, 41.

Ashton,F., and Wolfendale,A.W., 1963, Proc.Phys.Soc., 81, 593.

Barsanti,G., Conversi,M., Focardi,S., Murtas,G.P., Rubbia,C., and Torrelli,G., 1956, Proc.Geneva Conf.

Baxter,A.J., Watson,A.A., and Wilson,J.G., 1966, Proc.London Conf. Cosmic Rays. To be published.

Bennett,H.W., and Nash,W.F., 1960, Nuovo Cim., 15, 193.

Bennett,S., and Greisen,K., 1961, Phys.Rev., 124, 1982.

Bhabha,H.J., and Heitler,W., 1937, Proc.Roy.Soc., A, 159, 432.

Brooke,G., Gardener, M., Lloyd,J.L., Kisdnasamy,S., and Wolfendale,A.W., 1962, Proc.Phys.Soc., 80, 674.

Bull,R.M., Nash,W.F., Rastin,B.C., 1965, Nuovo Cim., 40, 348.

Carlson,J.F., and Oppenheimer,J.R., 1937, Phys.Rev, 51, 220.

Caro,D.E., Parry,J.K., and Rathgeber,H.D., 1951, Aust.J.Sci.Res.A, 4,16.

Chatterjee,B.K., Lal,S., Matano,T., Murthy,G.T., Naranan,S., Sivaprasad,K., Sreekantan,B.K., Srinivasa Rao,M.V., and Vishwanath,P.R., 1966, Proc.London Conf.Cosmic Rays. To be published.

Ciok,P., Coghen,T., Gierula,J., Holynski,R., Jurak,A., Miesowicz,M., and Saniewska,T., 1958, Nuovo Cim., 10, 741.

Clark,G., Earl,J., Kraushaar,W., Linsley,J., Rossi,B.B., and Scherb,F., 1958, Nuovo Cim., 8, Suppl.2, 623.

Jones,D.G., Taylor,F.E., and Wolfendale, A.W., 1962, Proc.Phys.Soc., 80, 686.

Kraushaar, W.L., and Marks,L.J., 1954, Phys.Rev., 93, 326.

Landau,L., 1953, Izv.Akad.Nauk.SSSR, Ser.Fiz., 17, 51.

Lilliorap,S.C., Wills,R.D., and Turver,K.E., 1963, Proc.Phys.Soc., 82, 95.

McCusker, C.B.A., 1963, Proc.Int.Conf.on Cosmic Rays, Jaipur, 4, 35.

Messel,H., and Potts,R.B., 1953, Nuovo Cim., 10, 754.

Messel,H., 1954, Progress in Cosmic Ray Physics, II, Ch.4.

Molière,G., 1946, Cosmic Radiation, Ed.W. Heidenberg.

Nishimwa,J., and Kamata,K., 1950, Prog.Theor.Phys., 5, 899.
1951, Prog.Theor.Phys., 6, 262, 628.
1952, Prog.Theor.Phys., 7, 185.

O'Connor,P.V., and Wolfendale,A.W., 1960, Nuovo Cim.(Suppl.2), 15, 202

Owen,B.G., and Wilson,J.G., 1955, Proc.Phys.Soc. A, 68, 409.

Pine,J., Davison,R.J., and Greisen,K., 1959, Nuovo Cim., 14, 1181.

Rochester,G.D., Somogyi,A.J., Turver,K.E., Walton,A.B., 1966, Proc.London Conf.Cosmic Rays. To be published.

Roe,B.P., and Ozaki,S., 1959, Phys.Rev., 116, 1022.

Rozental,I.L., 1952, Zh. Eksp. Teor. Fiz., 23, 440.

Snyder, H.S., 1949, Phys.Rev., 76, 1563.

Turver,K.E., 1963, Ph.D. Thesis, University of Leeds.

Ueda,A., and McCusker, C.B.A., 1962, Nuovo Cim., 6, 735.

Vernov,S.N., Tupolev,V.I., Khrenov,B.A., and Khristiansen,G.B.,1960, Proc.Moscow Conf.Cosmic Rays,II,158

Waddington,C.J., 1962, J.Phys.Soc.Japan,17, Suppl.A3,63.

Wilson,J.G., Allan,H.R., Lillicrap,S.C., Reid,R.J.O., and Turver,K.E., 1963. Proc.Jaipur Conf.Cosmic Rays, 4, 27.

Zatsepin,G.T., 1956, Proc.Oxford Conf.Extensive Air Showers, 8.
1960, Proc.Moscow Conf.Cosmic Rays, II, 1962.
1963, Proc.Jaipur Conf.Cosmic Rays, 4, 313.

ACKNOWLEDGMENTS

I am indebted to Professor G.D.Rochester F.R.S., for the provision of the facilities which have made this work possible and for his interest at all times.

I am most grateful to Dr. K.E.Turver for his continued encouragement and advice and for many valuable discussions on all aspects of the work.

I also wish to thank Professor J.G. Wilson and the members of the University of Leeds air shower group for the provision of the EAS data.

The contributions of Professor A.J. Somogyi and Mr. K.J. Orford to the analysis of the data are acknowledged with thanks.

The technical staff of the Physics Department, in particular Mr. W.Leslie and Miss A. Bevils, are thanked for their willing assistance.

Finally, my thanks are due to Mrs. H.Egerton whose patience in producing this typescript is much appreciated.